AD-A060 432 SYSTEMS SCIENCE AND SOFTWARE LA JOLLA CALIF F/G 14/2
DEVELOPMENT OF AIRBLAST AND THERMAL RADIATION INSTRUMENTATION.(U)
MAR 78 H R KRATZ, P L COLEMAN, R S WILSON DNA001-76-C-0365
UNCLASSIFIED SSS-R-78-3635 DNA-4594F NL

1 OF 1
AD A060 432

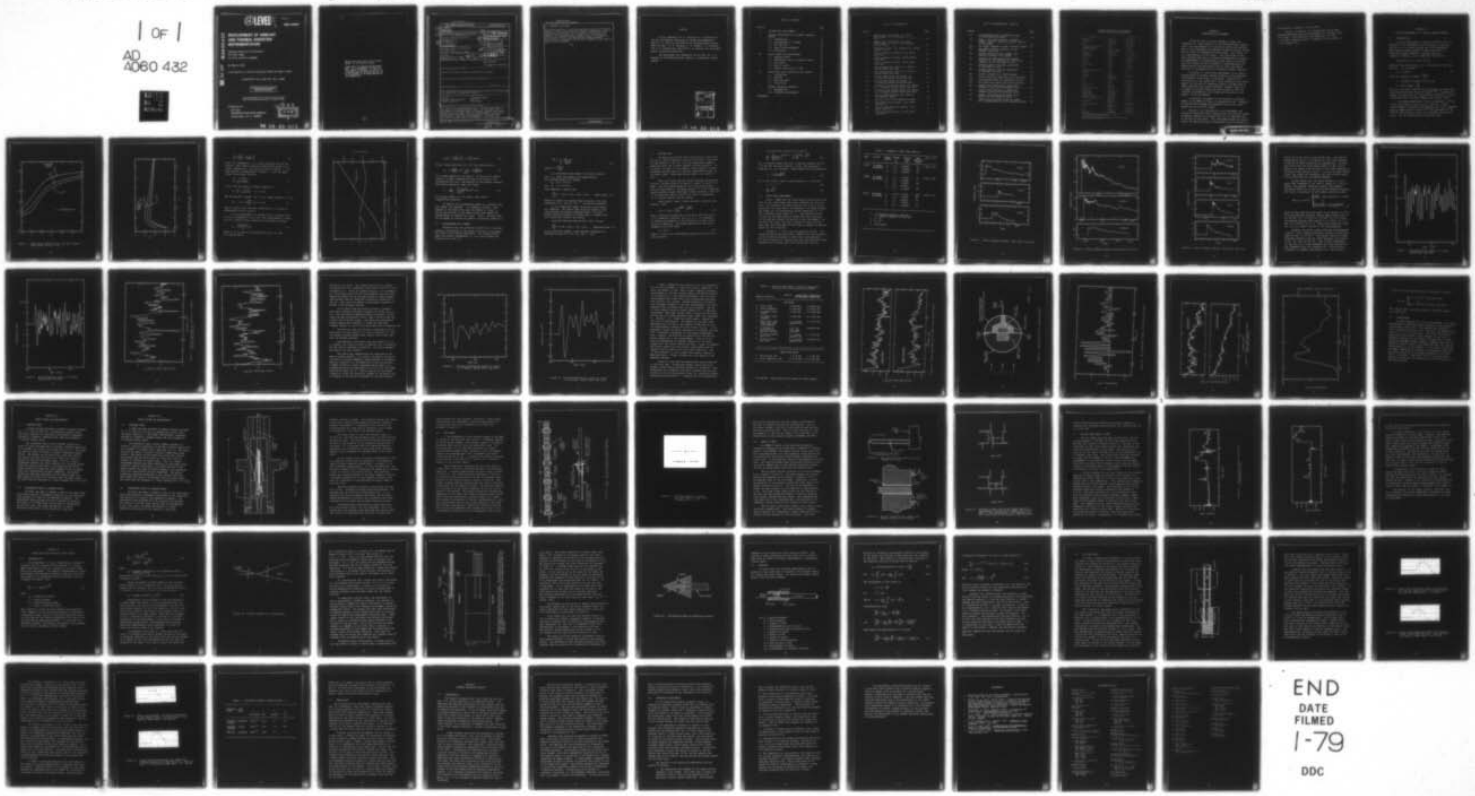

END
DATE FILMED
1-79
DDC

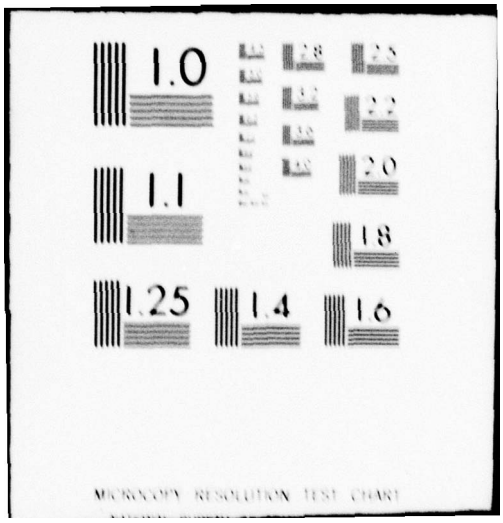
1.0
1.1
1.25
1.4
1.6
2.0
1.8
MICROCOPY RESOLUTION TEST CHART

(12) LEVEL II

DNA 4594F

DEVELOPMENT OF AIRBLAST AND THERMAL RADIATION INSTRUMENTATION

Systems, Science and Software
P.O. Box 1620
La Jolla, California 92038

31 March 1978

Final Report for Period 16 August 1976—31 March 1978

CONTRACT No. DNA 001-76-C-0365

APPROVED FOR PUBLIC RELEASE;
DISTRIBUTION UNLIMITED.

THIS WORK SPONSORED BY THE DEFENSE NUCLEAR AGENCY
UNDER RDT&E RMSS CODE B344077462 J11AAXSX35247 H2590D.

Prepared for
Director
DEFENSE NUCLEAR AGENCY
Washington, D. C. 20305

Destroy this report when it is no longer needed. Do not return to sender.

PLEASE NOTIFY THE DEFENSE NUCLEAR AGENCY, ATTN: TISI, WASHINGTON, D.C. 20305, IF YOUR ADDRESS IS INCORRECT, IF YOU WISH TO BE DELETED FROM THE DISTRIBUTION LIST, OR IF THE ADDRESSEE IS NO LONGER EMPLOYED BY YOUR ORGANIZATION.

UNCLASSIFIED

SECURITY CLASSIFICATION OF THIS PAGE (When Data Entered)

REPORT DOCUMENTATION PAGE

READ INSTRUCTIONS BEFORE COMPLETING FORM

1. REPORT NUMBER: DNA 4594F
2. GOVT ACCESSION NO.:
3. RECIPIENT'S CATALOG NUMBER:
4. TITLE (and Subtitle): DEVELOPMENT OF AIRBLAST AND THERMAL RADIATION INSTRUMENTATION
5. TYPE OF REPORT & PERIOD COVERED: Final Report, 16 Aug 76—31 Mar 78
6. PERFORMING ORG. REPORT NUMBER: SSS-R-78-3635
7. AUTHOR(s): H. R. Kratz, P. L. Coleman, R. S. Wilson
8. CONTRACT OR GRANT NUMBER(s): DNA 001-76-C-0365
9. PERFORMING ORGANIZATION NAME AND ADDRESS: Systems, Science and Software, P.O. Box 1620, La Jolla, California 92038
10. PROGRAM ELEMENT, PROJECT, TASK AREA & WORK UNIT NUMBERS: Subtask J11AAXSX352-47
11. CONTROLLING OFFICE NAME AND ADDRESS: Director, Defense Nuclear Agency, Washington, D.C. 20305
12. REPORT DATE: 31 March 78
13. NUMBER OF PAGES: 78
14. MONITORING AGENCY NAME & ADDRESS (if different from Controlling Office):
15. SECURITY CLASS (of this report): UNCLASSIFIED
15a. DECLASSIFICATION/DOWNGRADING SCHEDULE:

16. DISTRIBUTION STATEMENT (of this Report)

Approved for public release; distribution unlimited.

17. DISTRIBUTION STATEMENT (of the abstract entered in Block 20, if different from Report)

62710H

18. SUPPLEMENTARY NOTES

This work sponsored by the Defense Nuclear Agency under RDT&E RMSS Code B344077462 J11AAXSX35247 H2590D.

19. KEY WORDS (Continue on reverse side if necessary and identify by block number)

Airblast
Airblast Instrumentation
Thermal Radiation
Drag Measurements
DABS S-2
Bar Gauges

20. ABSTRACT (Continue on reverse side if necessary and identify by block number)

This is part of a continuing effort to develop instrumentation for use in underground nuclear tests. In particular, the development of instrumentation to measure airblast and thermal radiation is described. The initial development of an instrumented sphere to measure dynamic pressure in the supersonic flow behind a blast front was completed. Experiments are described that show that it is feasible to use a bar gauge → next page

DD FORM 1 JAN 73 1473 EDITION OF 1 NOV 65 IS OBSOLETE

UNCLASSIFIED

SECURITY CLASSIFICATION OF THIS PAGE (When Data Entered)

388 507

20. ABSTRACT (Continued)

to measure pressure on a surface parallel to the axis of the bar gauge by using a piston and fluid coupling combination. Work is described on sputtering a thin (2 micron) insulating film of sapphire onto the surface of a copper disc. Such films are required in a proposed thermal radiation gauge to measure the total radiation flux in an underground nuclear explosion. Measurements of pressure in the HE driver chamber on the DABS S-2 Test are also described.

PREFACE

We are indebted to D. R. Grine and J. R. Barthel for helpful discussions concerning air blast instrumentation and to W. G. Ginn for his efforts in fielding gauges on the DABS S-2 Test. B. S. Flanagan, R. W. Gilkey, F. I. Peterson and L. R. Prasser were very helpful in carrying out the experimental program reported here.

The assistance and cooperation of our COR, Mr. T. E. Kennedy of the Defense Nuclear Agency, is gratefully acknowledged.

TABLE OF CONTENTS

LIST OF ILLUSTRATIONS

LIST OF ILLUSTRATIONS (cont'd)

Conversion factors for U.S. customary to metric (SI) units of measurement.

To Convert From	To	Multiply By
angstrom	meters (m)	1.000 000 X E -10
atmosphere (normal)	kilo pascal (kPa)	1.013 25 X E +2
bar	kilo pascal (kPa)	1.000 000 X E +2
barn	meter^2 (m^2)	1.000 000 X E -28
British thermal unit (thermochemical)	joule (J)	1.054 350 X E +3
calorie (thermochemical)	joule (J)	4.184 000
cal (thermochemical)/cm^2	mega joule/m^2 (MJ/m^2)	4.184 000 X E -2
curie	*giga becquerel (GBq)	3.700 000 X E +1
degree (angle)	radian (rad)	1.745 329 X E -2
degree Fahrenheit	degree kelvin (K)	$t_K = (t°f + 459.67)/1.8$
electron volt	joule (J)	1.602 19 X E -19
erg	joule (J)	1.000 000 X E -7
erg/second	watt (W)	1.000 000 X E -7
foot	meter (m)	3.048 000 X E -1
foot-pound-force	joule (J)	1.355 818
gallon (U.S. liquid)	meter^3 (m^3)	3.785 412 X E -3
inch	meter (m)	2.540 000 X E -2
jerk	joule (J)	1.000 000 X E +9
joule/kilogram (J/kg) (radiation dose absorbed)	Gray (Gy)	1.000 000
kilotons	terajoules	4.183
kip (1000 lbf)	newton (N)	4.448 222 X E +3
kip/inch^2 (ksi)	kilo pascal (kPa)	6.894 757 X E +3
ktap	newton-second/m^2 (N-s/m^2)	1.000 000 X E +2
micron	meter (m)	1.000 000 X E -6
mil	meter (m)	2.540 000 X E -5
mile (international)	meter (m)	1.609 344 X E +3
ounce	kilogram (kg)	2.834 952 X E -2
pound-force (lbs avoirdupois)	newton (N)	4.448 222
pound-force inch	newton-meter (N-m)	1.129 848 X E -1
pound-force/inch	newton/meter (N/m)	1.751 268 X E +2
pound-force/foot^2	kilo pascal (kPa)	4.788 026 X E -2
pound-force/inch^2 (psi)	kilo pascal (kPa)	6.894 757
pound-mass (lbm avoirdupois)	kilogram (kg)	4.535 924 X E -1
pound-mass-foot^2 (moment of inertia)	kilogram-meter^2 (kg-m^2)	4.214 011 X E -2
pound-mass/foot^3	kilogram/meter^3 (kg/m^3)	1.601 846 X E +1
rad (radiation dose absorbed)	**Gray (Gy)	1.000 000 X E -2
roentgen	coulomb/kilogram (C/kg)	2.579 760 X E -4
shake	second (s)	1.000 000 X E -8
slug	kilogram (kg)	1.459 390 X E +1
torr (mm Hg, 0° C)	kilo pascal (kPa)	1.333 22 X E -1

*The becquerel (Bq) is the SI unit of radioactivity; 1 Bq = 1 event/s.
**The Gray (Gy) is the SI unit of absorbed radiation.

A more complete listing of conversions may be found in "Metric Practice Guide E 380-74," American Society for Testing and Materials.

SECTION I
INTRODUCTION AND SUMMARY

During the last few years Systems, Science and Software (S^3), under contract to the Defense Nuclear Agency (DNA), has participated in a continuing review and development of the techniques for measuring transient motion, stress and air blast in underground nuclear tests. This report is on a continuation of that effort. The objectives of the work reported here were to develop instrumentation suitable for measurements in underground nuclear tests in cavities, with the highest priority assigned to instrumentation for measuring gas flow associated with air blast and second priority to instrumentation for measuring thermal radiation.

In Section 2, the initial development of an instrumented sphere to measure dynamic pressure in the supersonic flow behind a blast front is described. Excitation of oscillations in the sphere was a major problem in this development; by the use of a composite sphere, the amplitude of these vibrations was greatly reduced. However, more work is needed to further reduce the oscillations so that the internal accelerometer, which measures the motion of the sphere, is not overranged.

In Section 3 we report on the fielding of pressure gauges in the DABS S-2 Tests, as requested by DNA. Pressure in the HE driver chamber was measured with two air blast gauges and two long bar gauges.

Section 4 is a discussion of the development and testing of piston and fluid couplings for use with bar gauges to measure pressure on surfaces that are not perpendicular to the axis of the gauge. This arrangement makes bar gauges useful for measuring static overpressure and the pressure on

the surfaces of wedges in an air blast.

Finally, in Section 5 we discuss work on the main problem associated with the development of a thermal radiation gauge. This problem is the deposition of a thin (2 micron) insulating layer of sapphire on the surface of a thin copper disc.

SECTION II

INITIAL DEVELOPMENT OF A DYNAMIC PRESSURE SENSOR

2.1 INTRODUCTION

A direct measurement of dynamic pressure, $\frac{1}{2}\rho u^2$, is important if the parameters, such as density ρ and flow velocity u, of a strong airblast are to be determined. Most pressure probes respond to some combination of static and dynamic pressure. The drag force on a sphere of radius r_s is an exception. This force is

$$\text{Drag Force} = F_D = C_D(\tfrac{1}{2}\rho_1 u_1^2)\pi r_s^2 \qquad (1)$$

where the drag coefficient, C_D, is a function of the flow velocity. In particular,

$$C_D = C_D(\text{Re},M) \qquad (2)$$

where Re = Reynold's number = $\dfrac{2u_1 r_s}{\nu_1}$,

ν_1 = kinematic viscosity of the gas,

M = Mach number = $\dfrac{u_1}{c_1}$,

and c_1 is the sound speed of the gas <u>behind</u> the blast front. If viscous forces are relatively small, i.e., the Reynold's number is larger than 10^4, then the drag coefficient is only a weak function of the Mach number (see Figures 1 and 2).

At standard temperature (20°C) and pressure (10^5 Pa, 1 bar), the viscosity of air is 0.15 cm^2/sec. A very limited amount of evidence (AIP Handbook, pp. 2-244) suggests that at temperatures of order 10^4°C and pressures of 1 kB (10^8 Pa) the viscosity is not very different from the STP value. For the strong shocks of interest here,

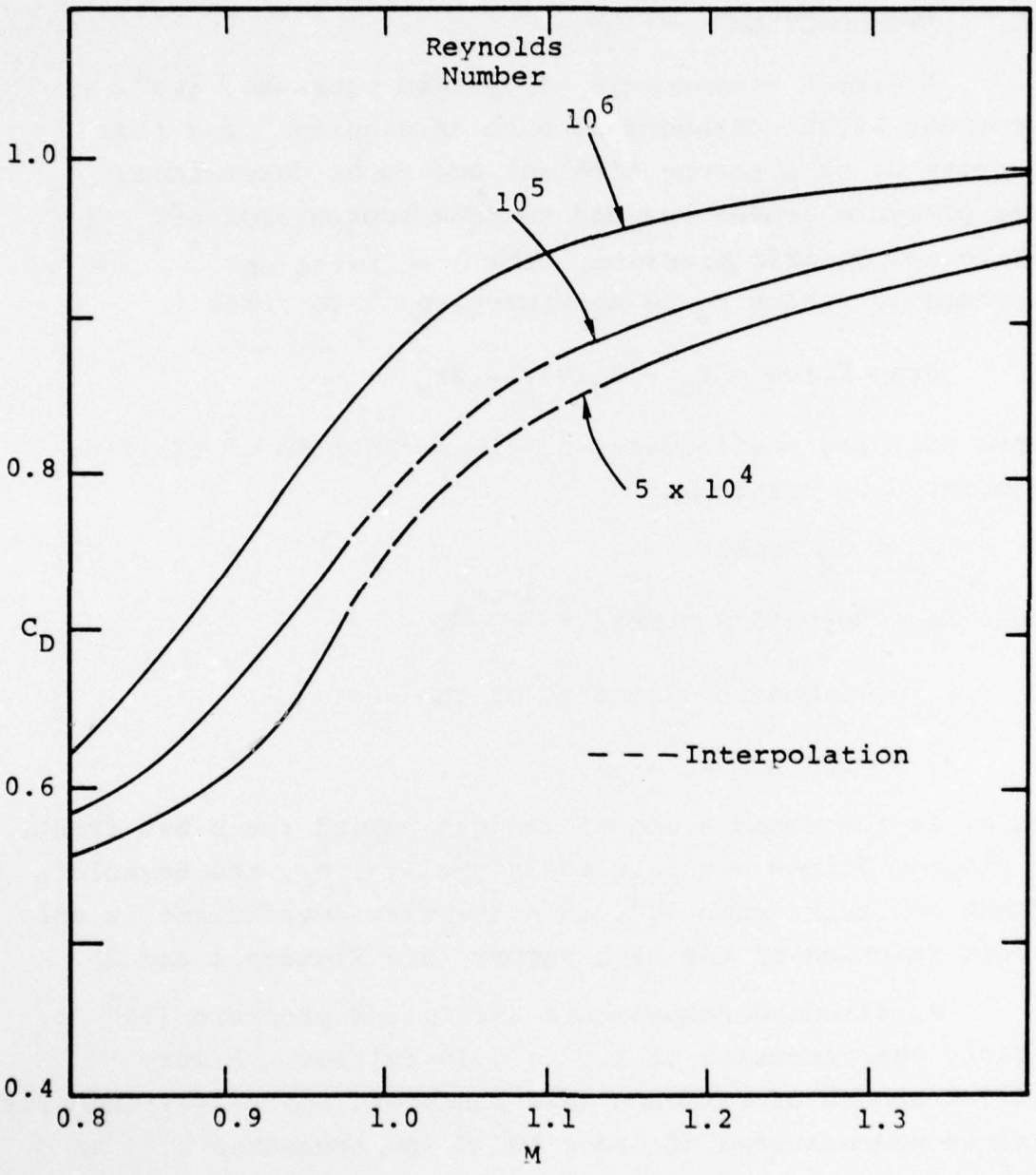

Figure 1. Sphere drag coefficient vs. flow Mach Number, M (from Bailey, et al., 1971).

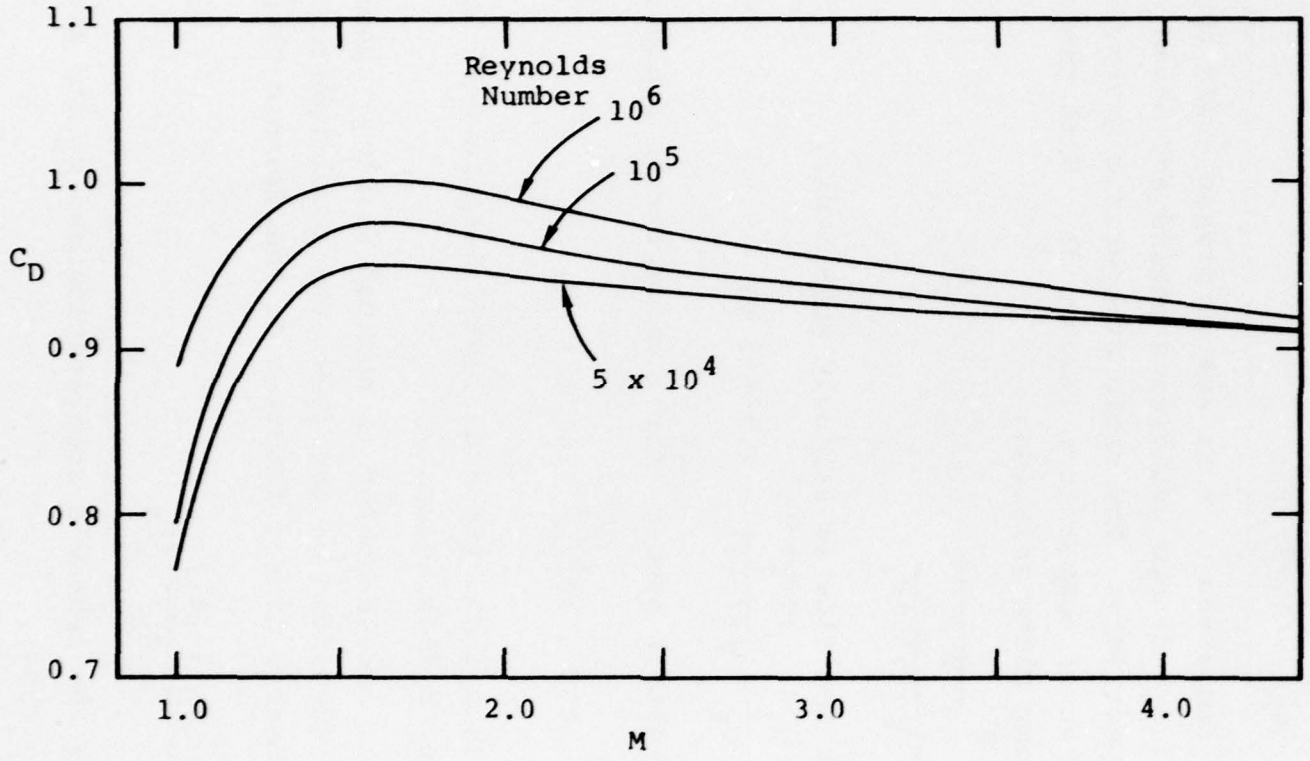

Figure 2. Sphere drag coefficient vs. flow Mach Number, M (cont.)
(from Bailey, et al., 1971).

$$\frac{T_1}{T_0} = \left(\frac{c_1}{c_0}\right)^2 = \frac{(\gamma-1)}{(\gamma+1)} \frac{P_1}{P_0} \tag{3}$$

where T is temperature, P is static pressure and the subscripts 1 and 0 denote quantities behind and ahead of the blast, respectively. The ratio of specific heats, γ, is a weak function of temperature (Figure 3). With the additional strong shock relation,

$$\frac{u_1}{c_0} = \sqrt{\frac{2\ P_1}{\gamma(\gamma+1)P_0}} \tag{4}$$

we see that the flow is strongly supersonic,

$$M = \frac{u_1}{c_1} = \sqrt{\frac{2}{\gamma(\gamma-1)}} \sim 2.9 \text{ @ 1 kB} \tag{5}$$

and the Reynold's number (for 1 cm or larger spheres) is high,

$$Re \sim 3.8 \times 10^5 \sqrt{\frac{P_1}{P_0}} \sim 10^7 \text{ @ 1 kB.} \tag{6}$$

Thus to within ±10%, the drag coefficient is 0.95 and is independent of flow velocity.

If an accelerometer is mounted within a sphere which in turn is suspended in the flow, the accelerometer's signal will be a nearly direct function of the dynamic pressure:

$$a_s = \frac{C_D\left(\frac{1}{2}\rho_1 u_1^2\right)}{m_s} \pi r_s^2 \tag{7}$$

where a_s is the sphere's acceleration and m_s its mass. In a strong shock,

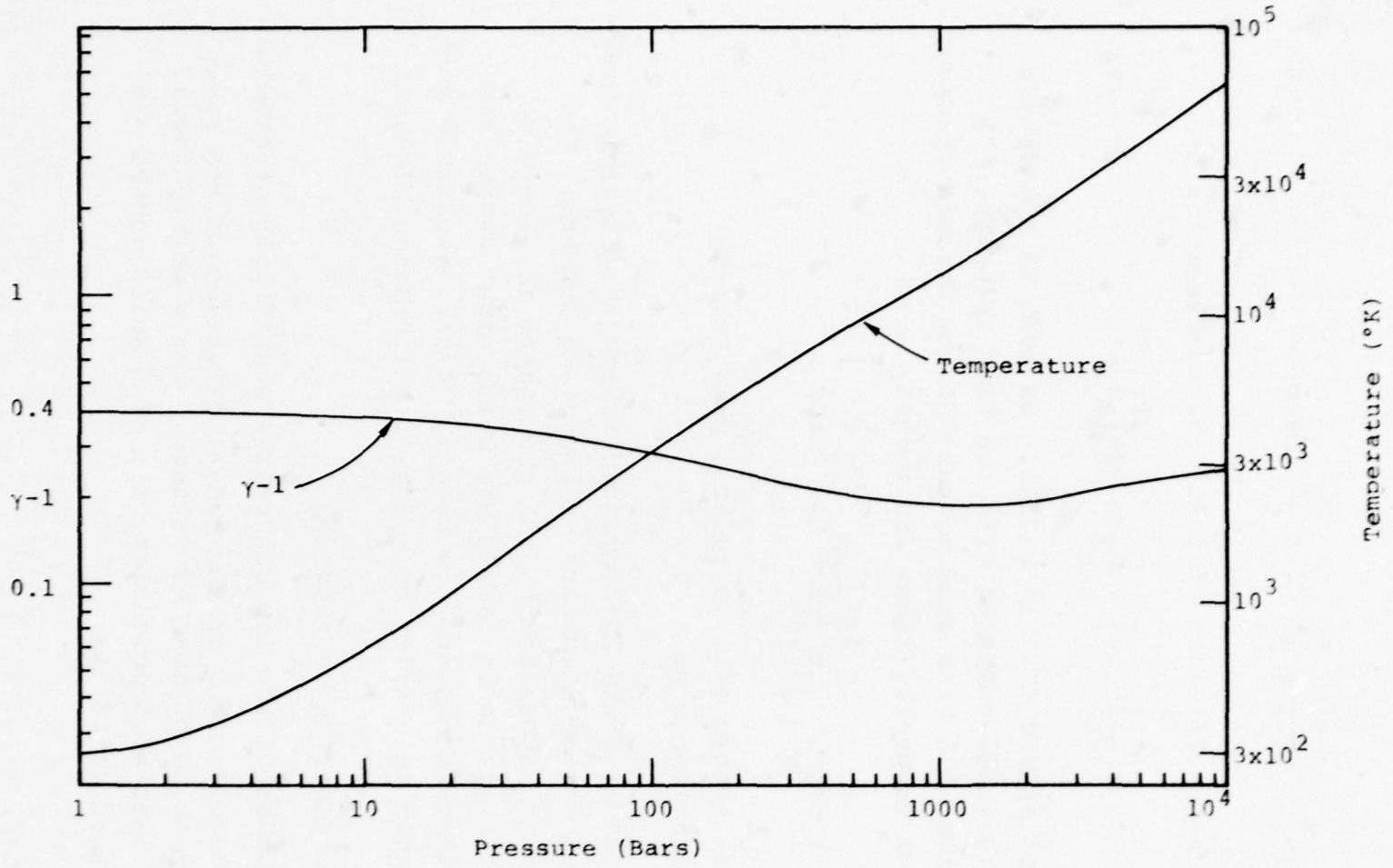

Figure 3. Temperature and γ vs. pressure for strong shocks in air.

$$\tfrac{1}{2}\rho_1 u_1^2 \sim \frac{\rho_0 c_0^4}{\gamma(\gamma-1)} \frac{P_1}{P_0} \sim 5.8 \frac{P_1}{P_0} \text{ (bars)}. \tag{8}$$

Using a drag coefficient of 0.95, the acceleration is

$$a_s \sim 3.5\left(\frac{P_1}{P_0}\right) \times 10^3 \frac{m}{sec^2} = 350\left(\frac{P_1}{P_0}\right) g's \tag{9}$$

for a steel sphere of 1 cm radius. As long as the sphere velocity is small compared with the flow velocity, the acceleration will be a good measure of the dynamic pressure. Thus useful measuring times are roughly

$$\Delta t \leq \frac{u_1}{10 a_s} \sim \frac{10.7\left(\rho_s r_s\right)}{\sqrt{P_1/P_0}} \times 10^{-4} \text{ sec} \tag{10}$$

For a steel sphere of 1 cm radius, this time is $8.6\sqrt{P_0/P_1}$ milliseconds.

To develop the instrumented sphere as a dynamic pressure probe, two problems are of immediate concern. The passage of the shock front past the sphere is likely to excite oscillations in the sphere which might damage the accelerometer or obscure its signal. Also, a suitable test bed is needed to confirm the gauge's calibration (Equation 7).

2.2 OSCILLATIONS OF A SPHERE

Because of the low cross-axis sensitivity of accelerometers, oscillations in the radial direction of the sphere are likely to be of most importance. For a purely radial mode, the natural frequencies, f_0, of a solid sphere are given by Love (1927) as

$$\tan x = \frac{x}{\left(1 - \frac{xc_p}{2c_s}\right)^2} \qquad (11)$$

where $x \equiv \frac{2\pi f_0 r_s}{c_p}$,

c_p = longitudinal wave speed in the sphere material,

and c_s = shear wave speed in the sphere material.

For the brass used in our spheres,

$c_p \sim 4.3 \times 10^3$ m/s

and $c_s \sim 2.1 \times 10^3$ m/s.

Thus, Equation 11 implies that

$$\frac{f_0 r_s}{c_p} = 0.440, 0.975, 1.484, 1.988, \ldots \text{ (Radial mode)} \qquad (12)$$

Spheres of radius 2.06 cm were readily available, for which resonances of 92, 204, 310, 415, ... KHz would be expected.

In the "spheroidal" modes, the motion is both radial and tangential. The lowest order gives the sphere an alternately prolate and oblate ellipsoidal shape. One might predict that the incidence of a plane wave on a sphere would also induce such a mode of oscillation.

Using the relations given by Love (1927), we find

$$\frac{f_0 r_s}{c_s} = 0.422, 0.816, 1.377, 1.964, \ldots \text{ (Spheroidal mode)} \qquad (13)$$

For our particular spheres, these resonant frequencies are predicted to occur at 43, 83, 140, 200, ... KHz.

2.3 THE TEST BED

An explosively driven shock tube offers a fairly simple way to achieve moderately strong blast waves (~100 bars) of long duration (~200 μs). The one-dimensional geometry makes efficient use of small amounts of high explosive. In our tests, we used 15.2 cm diameter "Burke tubing" (a heavy cardboard cylinder used for concrete construction forms) as the shock tubes. These were buried under ½ to 1 meter of soil.

Each air-filled tube was driven from one end by sheet HE with a surface density of about 0.5 gm/cm^2 (1 lb/ft^2) of PETN. With the charge backed up by a thick steel plate, this was equivalent to an energy source of 3×10^7 Joules/ms^2. Quartz pressure gauges (PCB Model 101A02) mounted in the wall of the tube were used to monitor the static overpressure, P_1, at various ranges from the charge.

Self-similar "blast" theory predicts (Cavaliere and Messina, 1976)

$$X(t) = K(g,s,\gamma)\left(\frac{E_0}{\rho_0}\right)^{\frac{1}{(g+2)}} t^{\frac{(s+2)}{(g+2)}} \qquad (14)$$

where X denotes the position of the shock front at time t, K is a numerical constant, and g is 1, 2, or 3 depending on whether the geometry of the explosion is plane, cylindrical or spherical. The energy deposited in the gas is assumed to be of the form

$$E = E_0 t^s \ , \qquad (15)$$

where s is zero for instantaneous deposition and one for a step function.

The shock front velocity is given by

$$\frac{dX}{dt} = \left(\left[\frac{(g+2)}{(s+2)} \right]^{-\frac{s}{2}(g+2)} \frac{E_0}{K\rho_0} \right)^{\frac{1}{(s+2)}} X^{\frac{s-g}{s+2}} \qquad (16)$$

For a classical shock tube with a constant pressure driver, s is one and the shock velocity, dX/dt, and the static pressure, P_1, are constant. These quantities are related by

$$P_1 = 2\frac{\rho_0}{(\gamma+1)}\left(\frac{dX}{dt}\right)^2 . \qquad (17)$$

For a true "blast" wave in plane geometry, g is one and

$$X \propto t^{2/3} E^{1/3} \qquad (18)$$

$$\frac{dX}{dt} \propto \sqrt{\frac{E_0}{X}} . \qquad (19)$$

2.4 SHOCK TUBE EXPERIMENTS

Table 1 summarizes the peak pressure and arrival time data for the three shock tube tests conducted for this project. The variation of shock position with time is fairly consistent for these tests; the exponent α is midway between the values for an instantaneous energy deposition (s = 0) and a constant power input (s = 1). The absolute values of position and peak pressure versus time vary from test to test and may reflect the quality of the containment; for the first two tests, the tube is buried in soil; for the last test, the first meter of the tube is encased in approximately 10 cm of concrete.

Figures 4, 5, and 6 show the pressure records. The structure behind the shock front suggests that the detonation of the explosive required at least tens of microseconds. The use of Equation 17 implies that the peak pressures should decrease with distance much less rapidly than they do.

Table 1. Summary of shock tube results.

Test	Source	Gauge Type[1]	Range (m)	Arrival Time (μs)	Peak Pressure (bars)	α[2]	β[3]
A2374	45 grams Primacord	P	1.0	4.6×10^2	~45	0.797	-1.11
		P	2.0	1.08×10^3	~23		
		P	3.0	1.83×10^3	~13		
A2380	89 grams Detasheet	P	1.0	3.2×10^2	~70	0.812	-0.81
		S	1.2	3.9×10^2	--		
		P	2.0	7.3×10^2	~45		
		S	2.2	8.2×10^2	--		
		P	3.0	1.24×10^3	~28		
A2412	89 grams Detasheet	P	0.505	1.4×10^2	~130[4]	0.839	-0.71
		P	1.0	2.9×10^2	~85		
		P	2.0	6.9×10^2	~55		
		S	2.2	7.9×10^2	--		
		P	3.0	1.15×10^3	~35		

1. P ≡ Pressure gauge in tube wall
   S ≡ Sphere suspended on tube axis
2. $X \propto t^{\alpha}$
3. $P \propto X^{\beta}$
4. First peak.

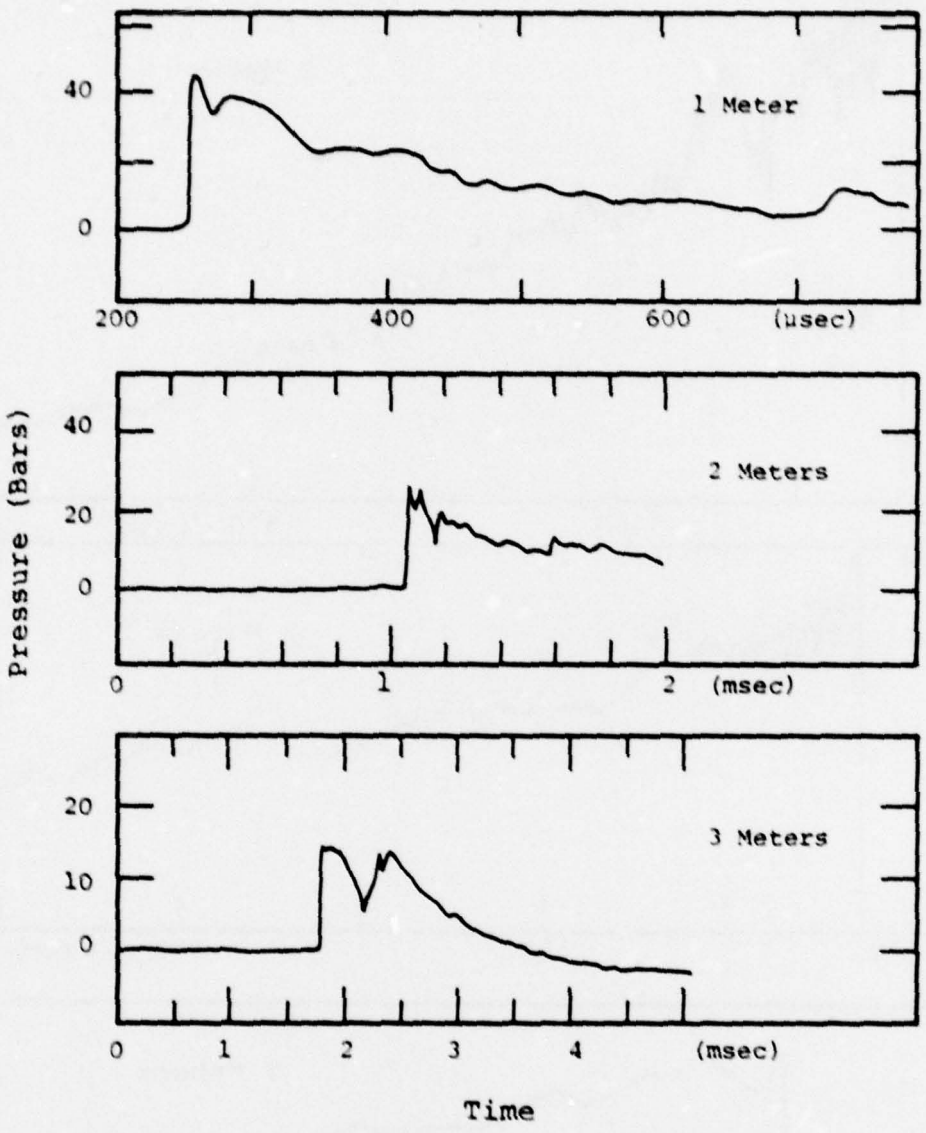

Figure 4. Static pressure records, first shock tube shot.

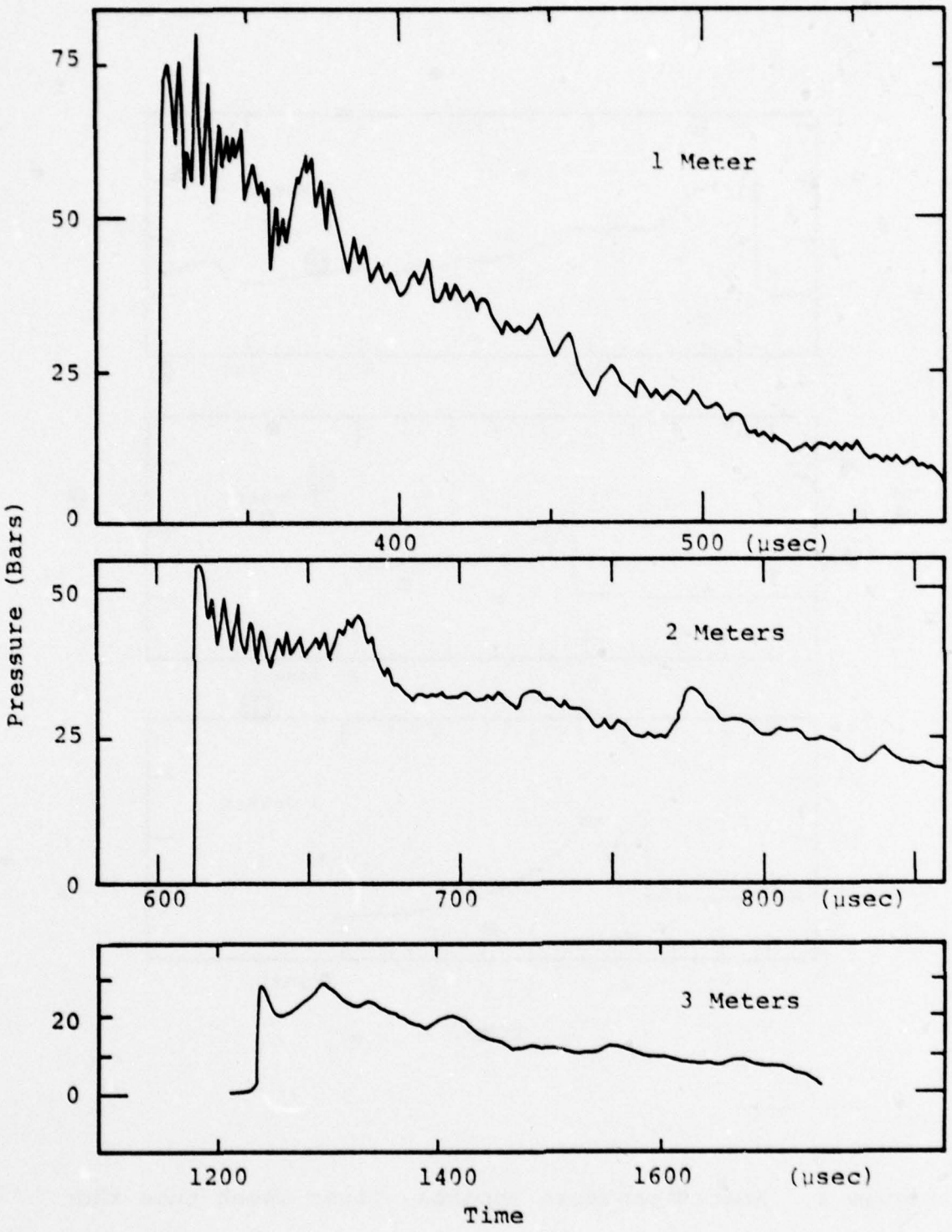

Figure 5. Static pressure records, second shock tube shot.

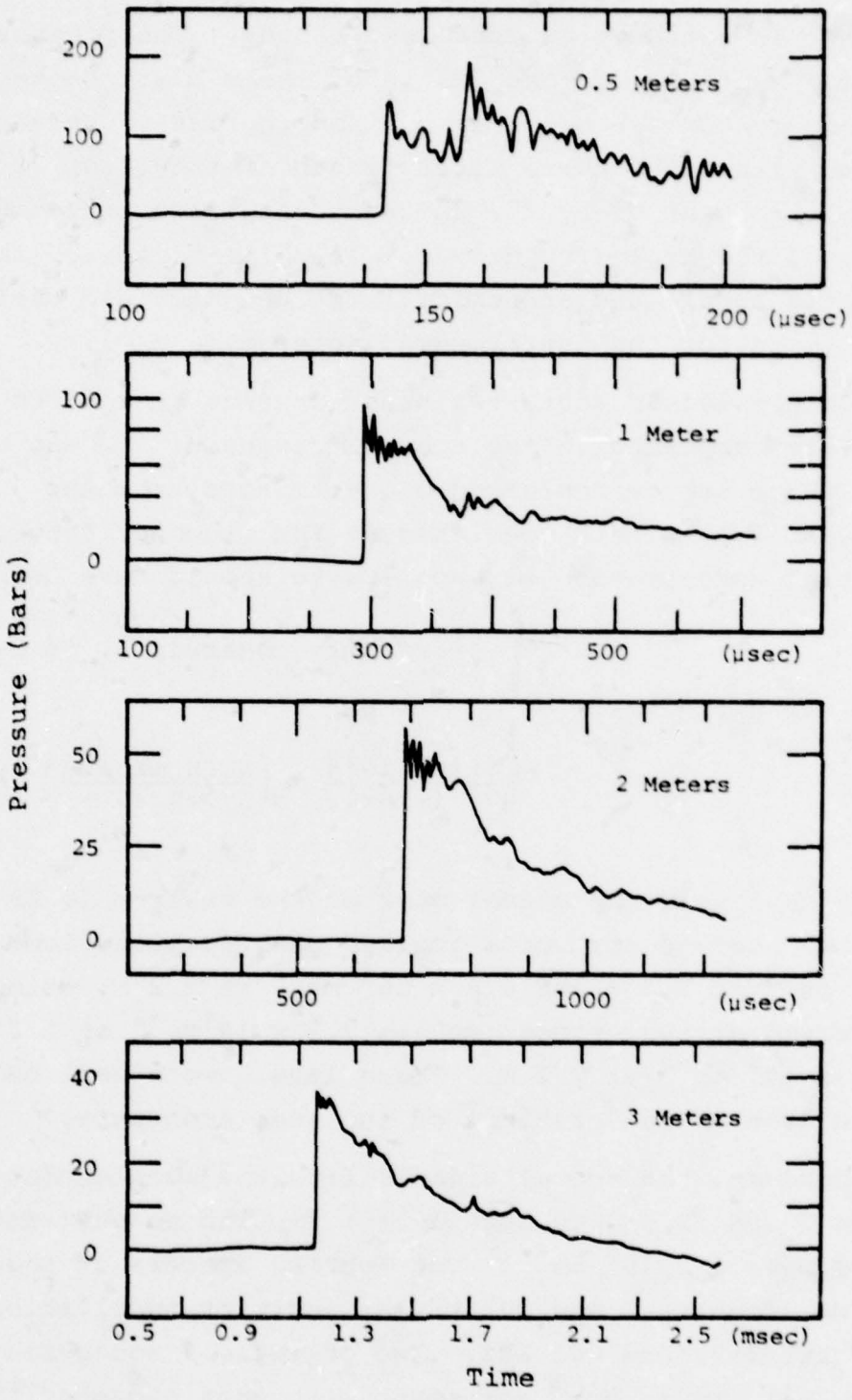

Figure 6. Static pressure records, third shock tube shot.

Clearly we do not have an ideal shock tube. The pressure gauges may be faulty in the design of their blast package or the use of Burke tubing may be inappropriate. We also note that within the three meter length of tube, the 70 grams of air swept up by the shock is not large compared to the mass of the explosive driver. In spite of these limitations, this simple and economical test bed provided useful initial tests for the instrumented spheres.

On the second shot, two brass spheres of 2.06 cm radius were suspended in the tube at ranges of 1.2 and 2.2 meters. Each sphere contained a quartz accelerometer (PCB Model 305A) with a specified 60 KHz resonant frequency. The initial acceleration of each sphere should have been

$$(\text{max } a_s \text{ in } m/s^2) \cong \begin{cases} \dfrac{410}{(\gamma-1)} \cdot (\text{max observed } P_1 \text{ in bars}) \\ \text{or} \\ \dfrac{1.1 \times 10^{10}}{(\gamma-1)(\gamma+1)} \alpha \left(\dfrac{X \text{ in meters}}{t \text{ in } \mu s}\right)^2 \end{cases} \quad (20)$$

where we have used the actual mass of the spheres (0.29 kg). Using the observed pressures implies peak accelerations of 8×10^4 ms^{-2} at 1.2 m and 4.6×10^4 ms^{-2} at 2.2 m; using the observed arrival times implies $9.2 \times 10^4 ms^{-2}$ at 1.2 m and 6.6×10^4 ms^{-2} at 2.2 m. These levels were well below the 5 to $10 \times 10^5 ms^{-2}$ ratings of the accelerometers.

However, the actual signals from the accelerometers (Figures 7 and 8) showed significant ringing to peak amplitudes of over 5×10^5 ms^{-2}. The Fourier spectra of these waveforms (Figures 9 and 10) reveal dominant oscillations at 38, ~90, 168, and 201 KHz. Two of these frequencies (90 and 201) are in good agreement with that expected for the fundamental and first harmonic of a uniform radial pulsation of a sphere (see Equation 12). The origin of

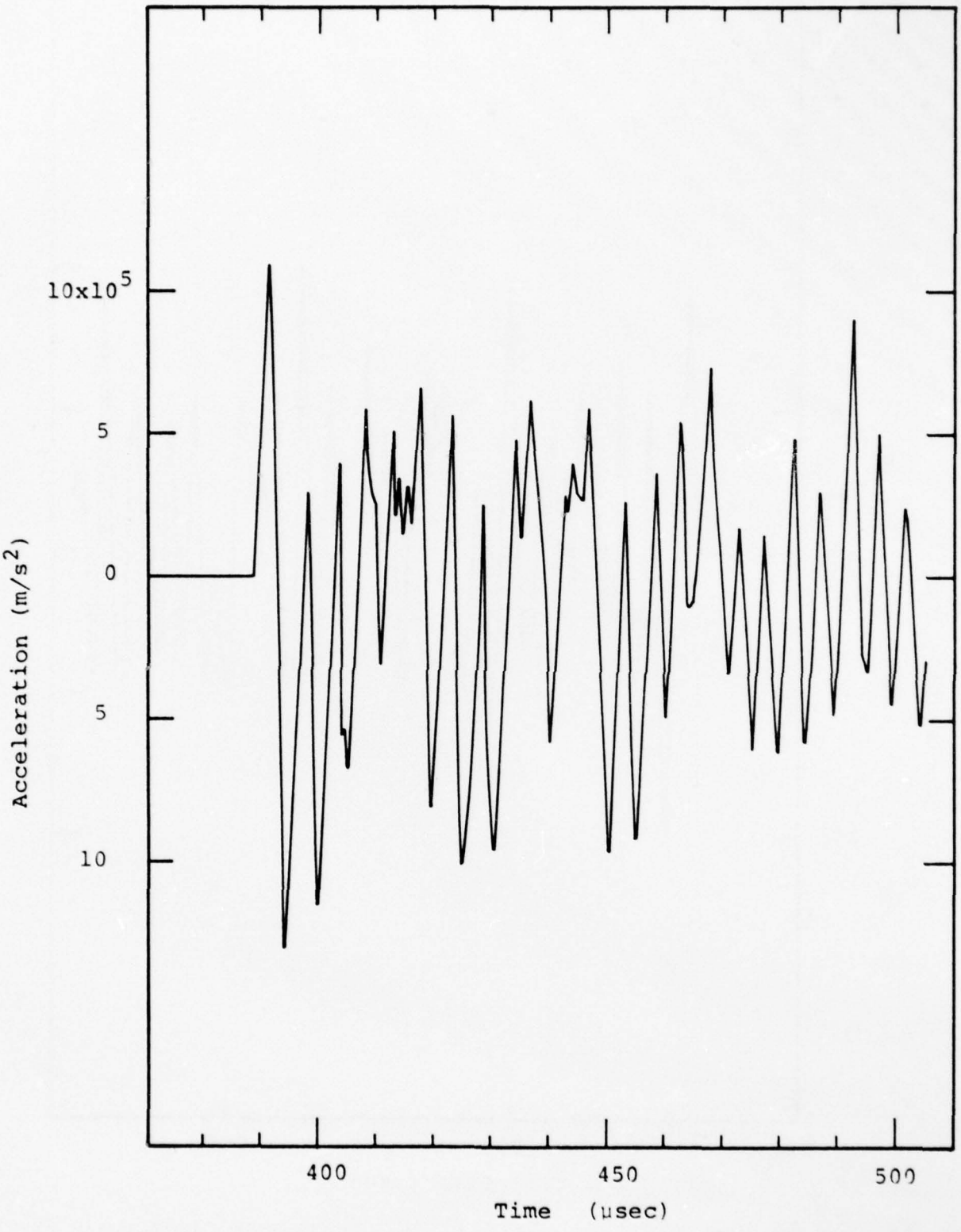

Figure 7. Raw acceleration signal @ 1.2 meters, second shock tube test.

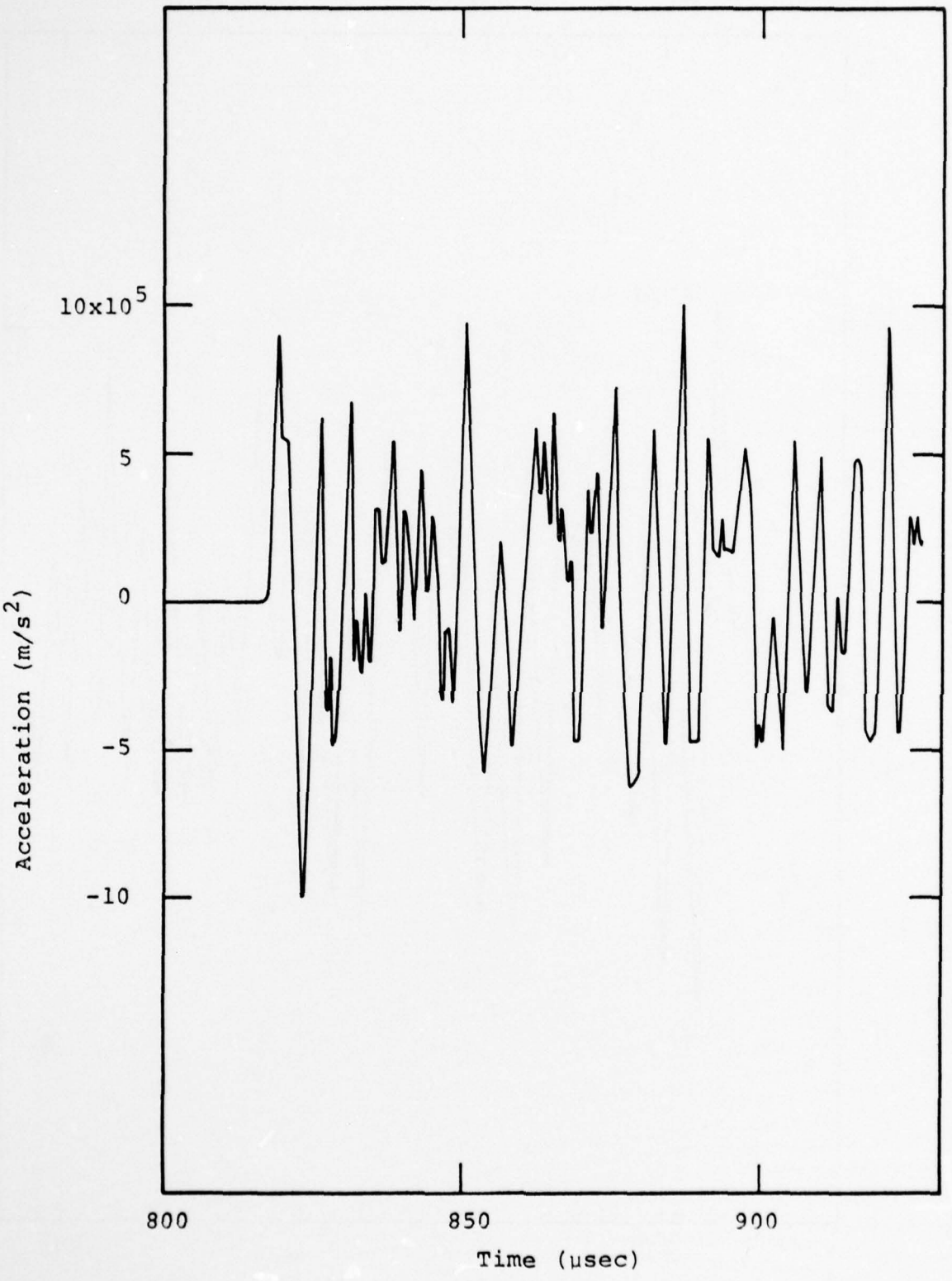

Figure 8. Raw acceleration signal @ 2.2 meters, second shock tube test.

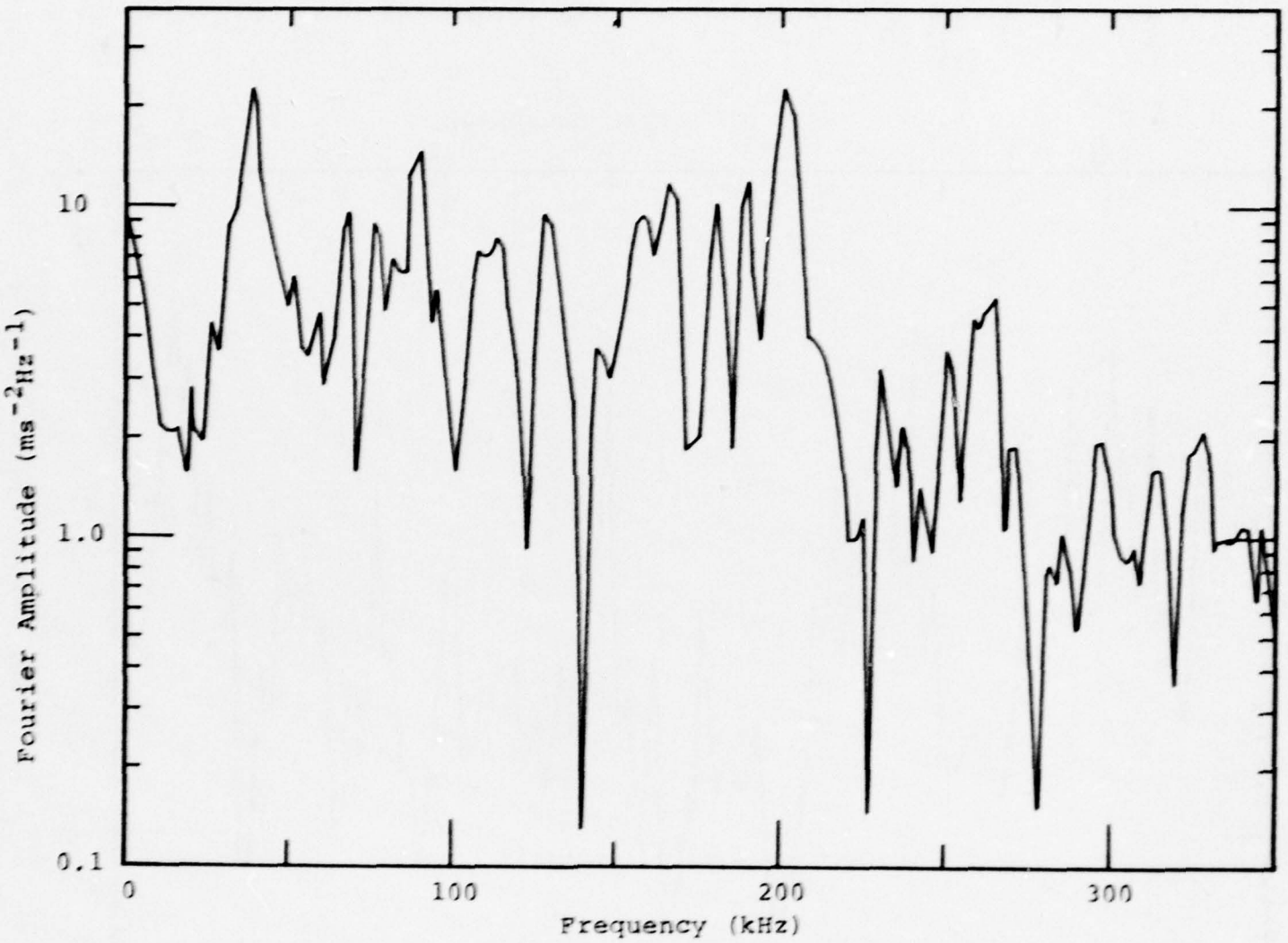

Figure 9. Fourier amplitudes for sphere at 1.2 meters, second shock tube shot.

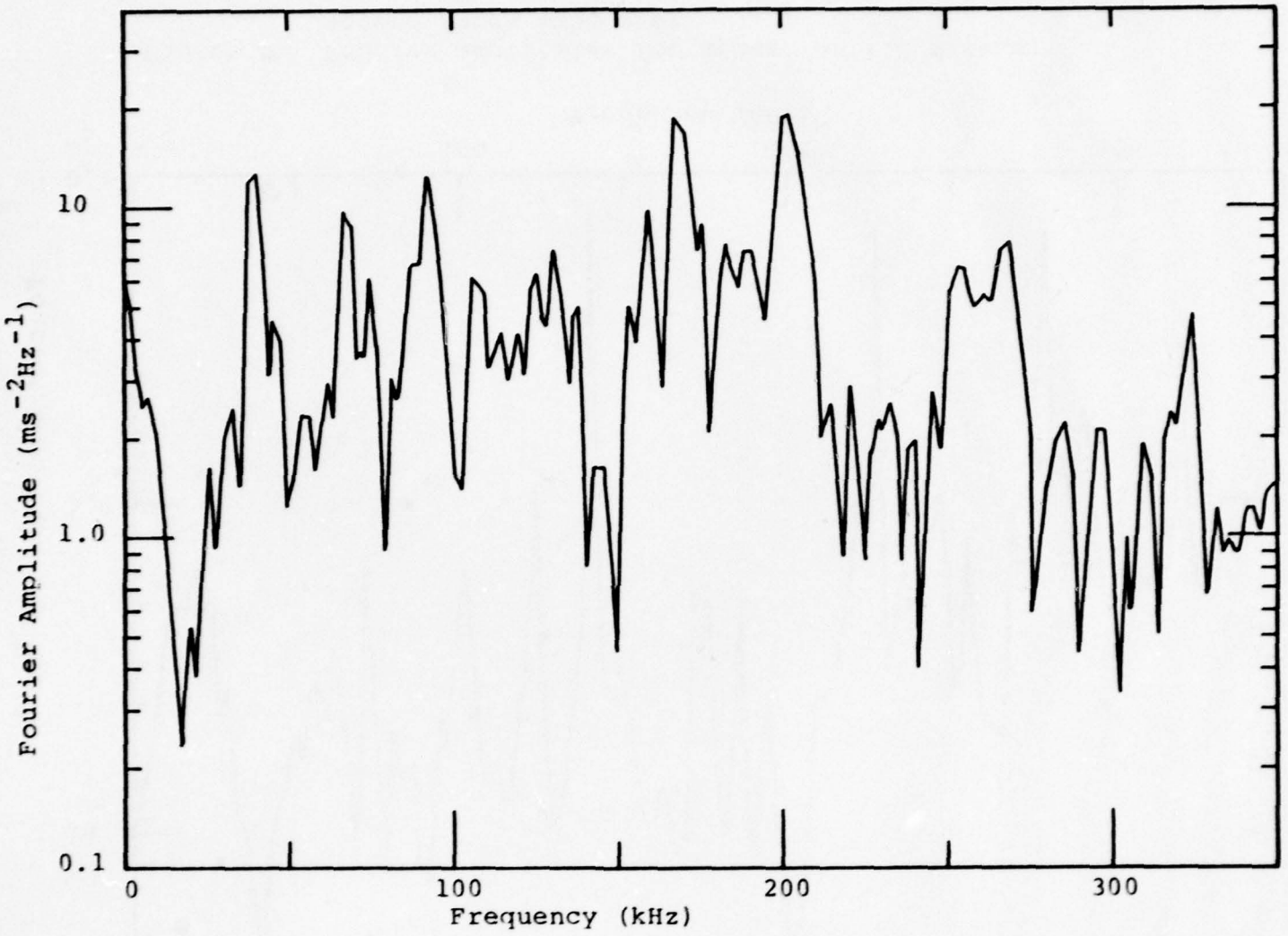

Figure 10. Fourier amplitudes for sphere at 2.2 meters, second shock tube shot.

168 KHz is not clear. The lowest oscillation is roughly coincident with the fundamental spheroidal oscillation given by Equation 13. Since the spheres contain 1.27 cm diameter by 2.78 cm deep holes for the accelerometers and the sound speeds for brass are not precisely known, we might expect some changes from the idealized frequencies (Equations 12 and 13). Note that the nominal accelerometer resonance at 60 KHz is not strongly excited.

If we unfold from the Fourier spectra a harmonic oscillator response (resonant frequency of 38 KHz and Q of 6.3), derived from the observed spectra, and apply a third order low pass Butterworth filter (down 3 db at 50 KHZ and rolling off 36 db per octave), the resulting acceleration signals appear more plausible in shape and amplitude (compare Figures 11 and 12 with the predictions of Equation 20).

The data are also qualitatively consistent with the prediction of blast theory (s is zero in Equation 15) that the dynamic pressure decays more rapidly (with time) than does the thermal pressure.

Unfortunately, the signal from the sphere at 1.2 m is suspect; the initial signal is positive, as it should be, but the overall waveform is negative. We have no adequate explanation for this problem.

The second shot demonstrated the magnitude of the sphere ringing problem. As a result, we began a series of lab tests on various composite configurations for a sphere, seeking a reduction in the magnitude of the oscillations. A hammer striking a freely suspended sphere gave it an acceleration pulse of magnitude (5-10) x 10^4 ms^{-2} and FWHM duration of about 100 μs. Fourier spectra of the pulses allowed us to see how structural changes in the sphere led to changes in the relative strengths of the oscillations.

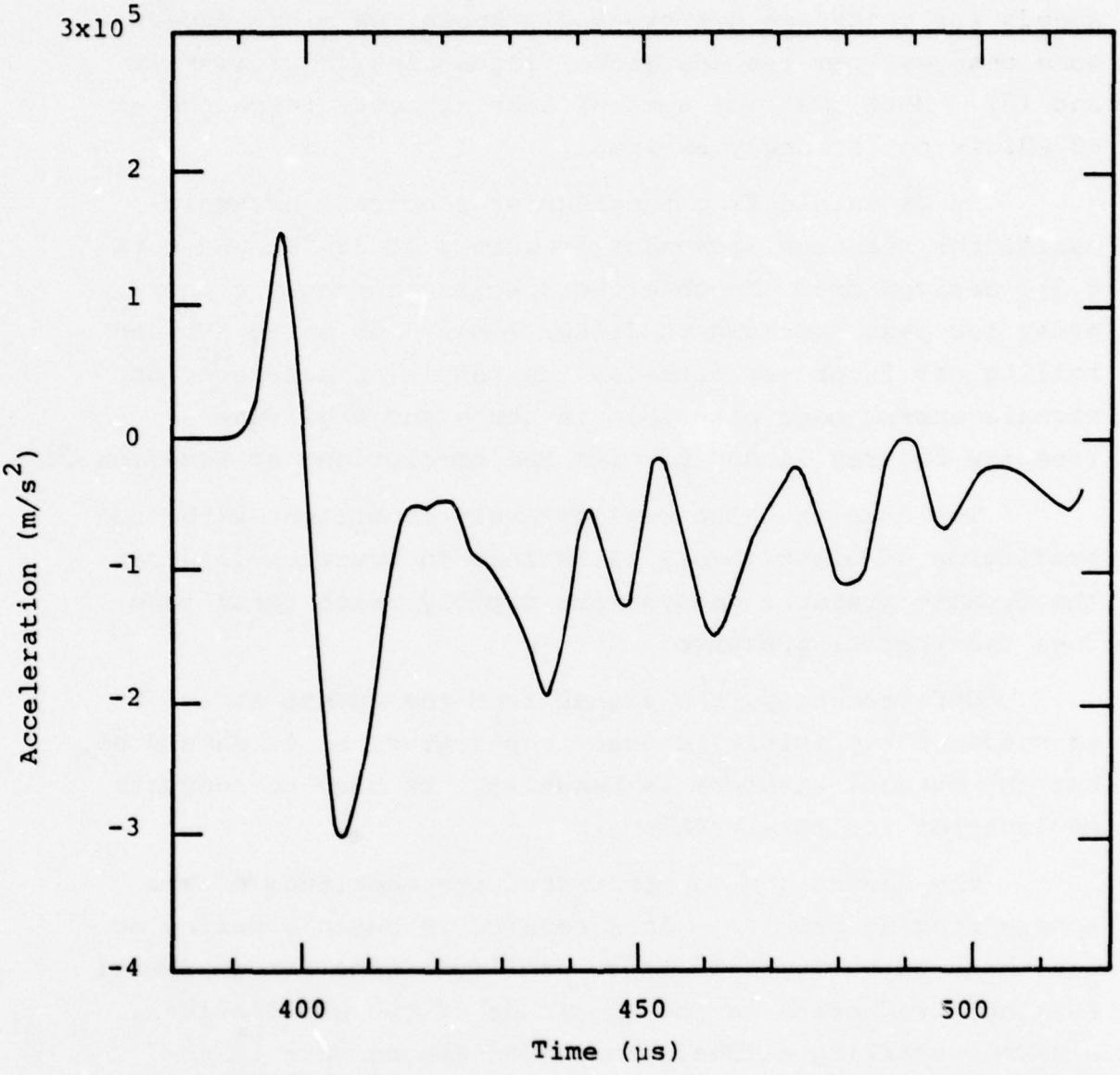

Figure 11. Filtered acceleration signal for sphere at 1.2 meters, second shock tube shot.

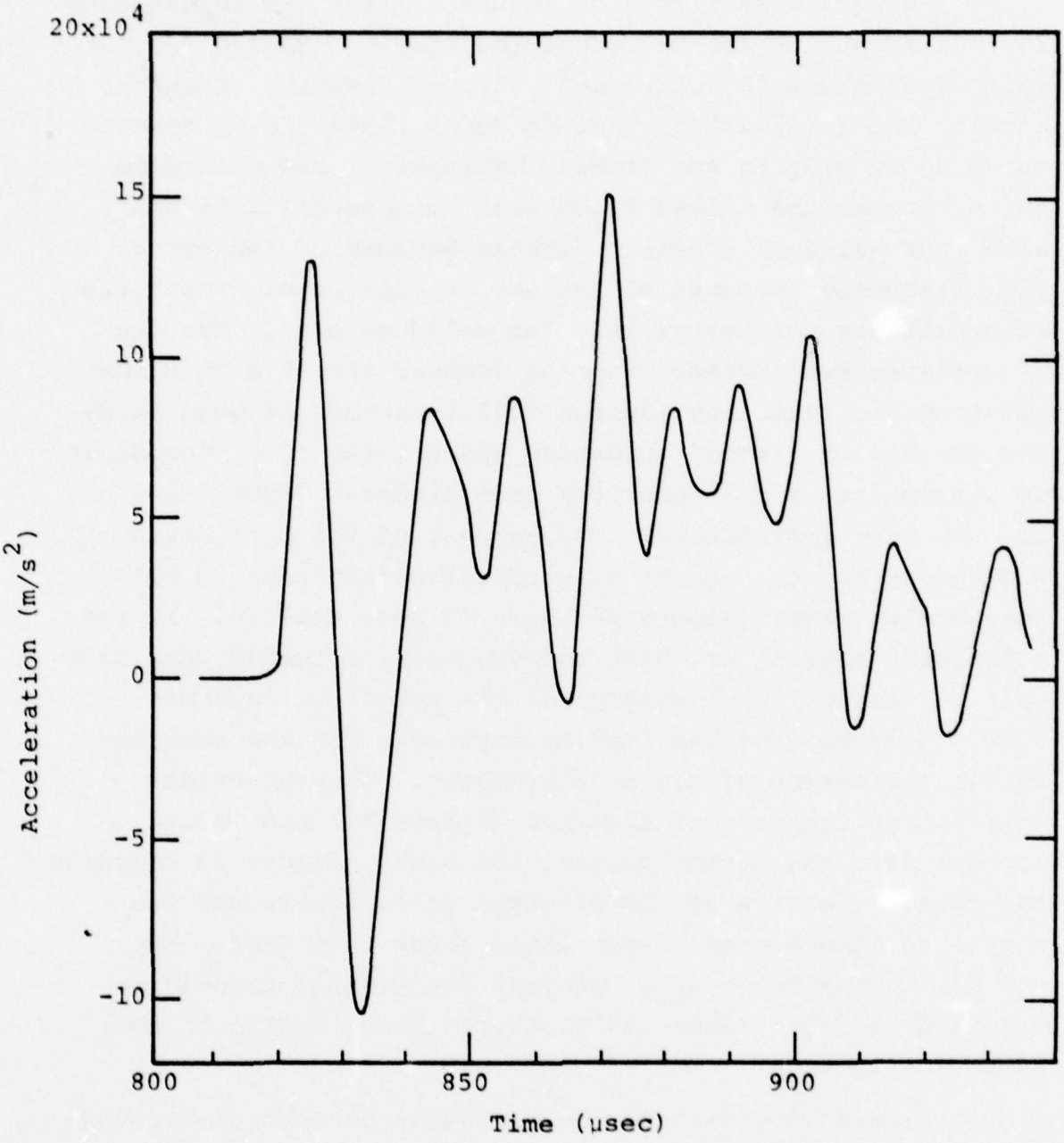

Figure 12. Filtered acceleration signal for sphere at 2.2 meters, second shock tube shot.

Table 2 summarizes the results of the lab experiments. For our first attempt to reduce the ringing (sphere #2), we split the sphere in half, used a higher resonant frequency accelerometer (>150 KHz, Endevco Model 2264A-50K-R) mounted on an epoxy plug in the forward hemisphere, and thin wood shims between the halves which were reconnected internally with four No. 8-32 screws. Perhaps because of the better high frequency response of the new accelerometer, the first composite was not better than the solid spheres. The use of nylon screws instead of brass (sphere #3), 0.4 mm thick elastromeric foam tape (Scotch Y4921) instead of wood shims and the use of a sound absorbing sheet (DYAD .050, Soundcoat Co., Brooklyn, N.Y.) under the accelerometer (sphere #4) did not help appreciably. The removal of the back brass hemisphere and the use of only adhesive foam tape to hold the accelerometer (sphere #6) were of most utility. In the supersonic regime for which the sphere is intended, the back half is probably unnecessary for the proper aerodynamic flow. However, the back may be important for the environmental protection of the accelerometer. Thus we tried trailing hemispheres of aluminum (sphere #7) and lucite (sphere #8), the latter proving the best. Figure 13 compares the Fourier spectra of the original solid sphere and the composite sphere used in our final shock tube test. The ~40 KHz resonance is still present but greatly reduced in magnitude and Q. Figure 14 shows the final design of the composite spheres.

Figure 15 gives the raw acceleration record observed in our third shot. Significant sphere ringing was still present as the Fourier spectrum (Figure 16) indicates. With corrections for a harmonic oscillator response and low pass filtering, the net acceleration signal is a plausible dynamic pressure record (Figure 17). Allowing for the reduced mass

Table 2. Relative magnitudes of Fourier components* for tests of various sphere structures.

Sphere Structure	Ratios: Amplitude @ Resonance / Low Frequency Amplitude	
	LAB TESTS	
1. Solid brass	0.4@38 KHz	0.02@200 KHz
2. First Composite	0.2@38 KHz	0.2 @200 KHz
3. #2 except Nylon screws	0.1@38 KHz	0.4 @200 KHz
4. #3 except sound absorber	0.1@38 KHz	0.1 @200 KHz
5. Front half only, foam tape under accelerometer	0.3, broad peak@60 KHz	0.3 @200 KHz
6. #5 except no accelerometer mounting screws	0.01, no real peak @~40 KHz	0.04@200 KHz
7. #6 plus aluminum back half	0.1, broad peak@40 KHz	0.1 @200 KHz
8. #6 plus lucite back half	0.01, broad peak@40 KHz	0.01@200 KHz
	SHOCK TUBE SHOTS	
1. Solid brass (#1)	~2 @ 40 KHz	~3 @ 200 KHz
2. Final composite (#8)	~0.3 @ 40 KHz	~0.2 @ 200 KHz

*In $m/s^2/Hz$. Power goes as the square of these numbers.

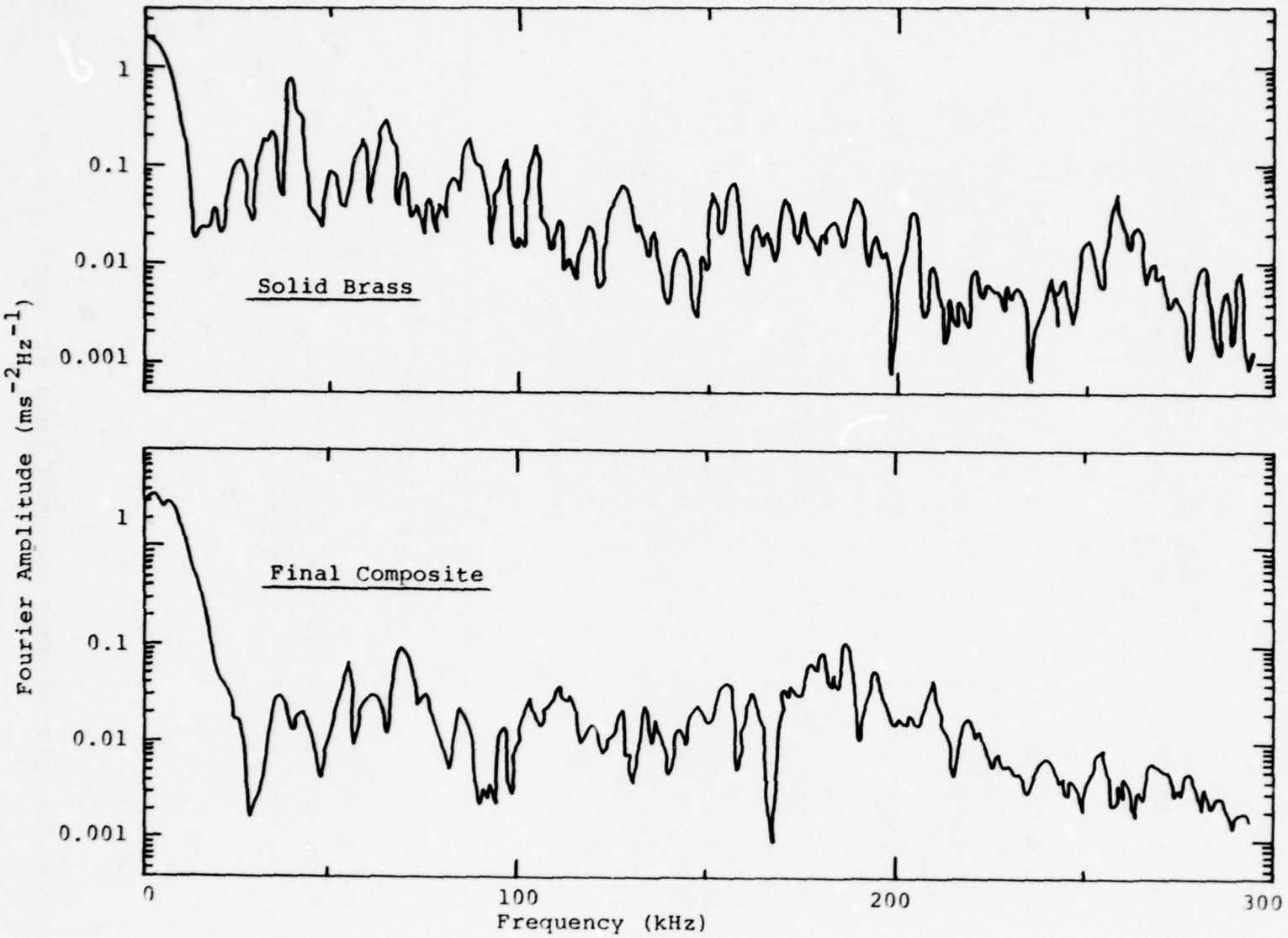

Figure 13. Fourier amplitudes for lab tests of two types of sphere.

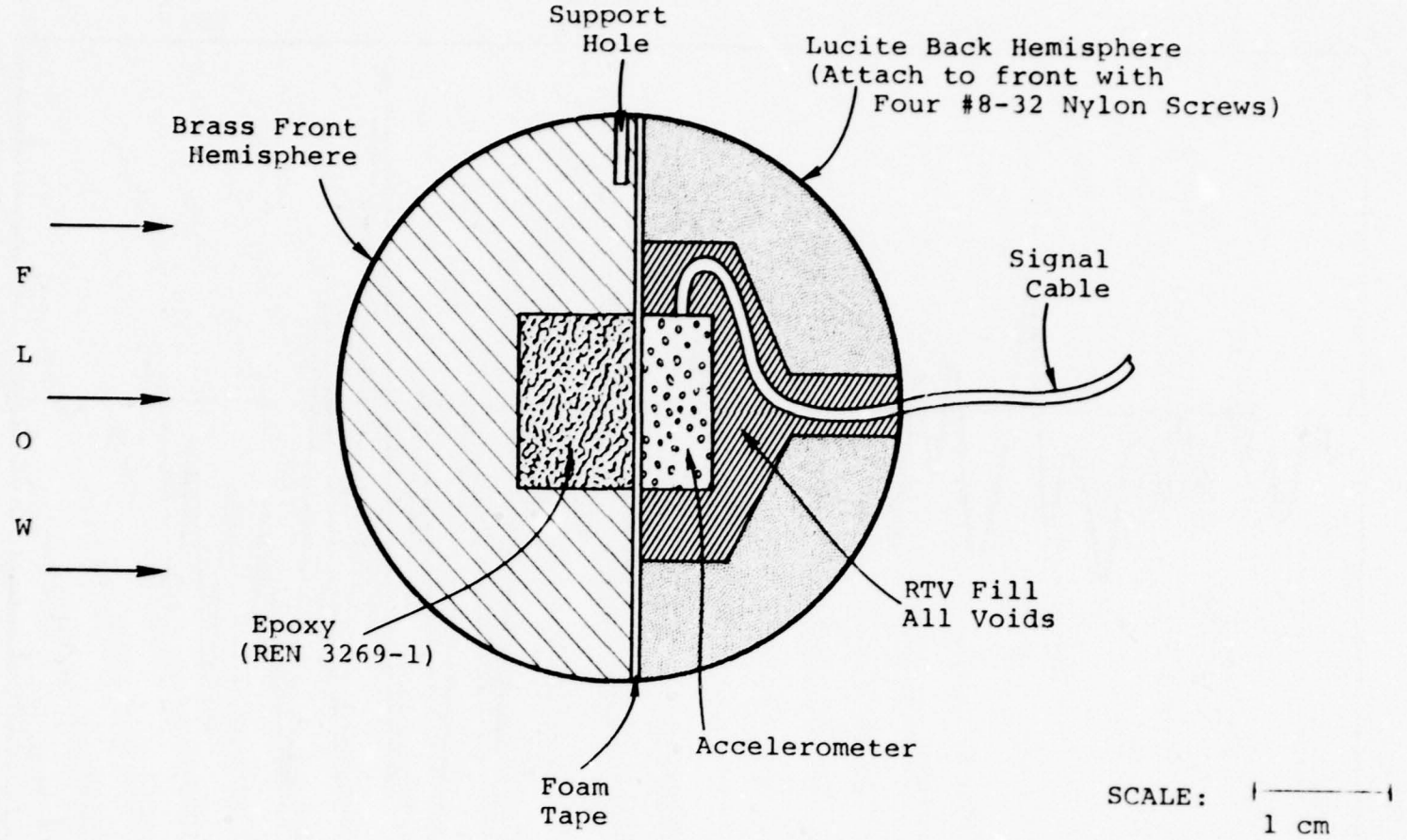

Figure 14. Section view of the composite sphere.

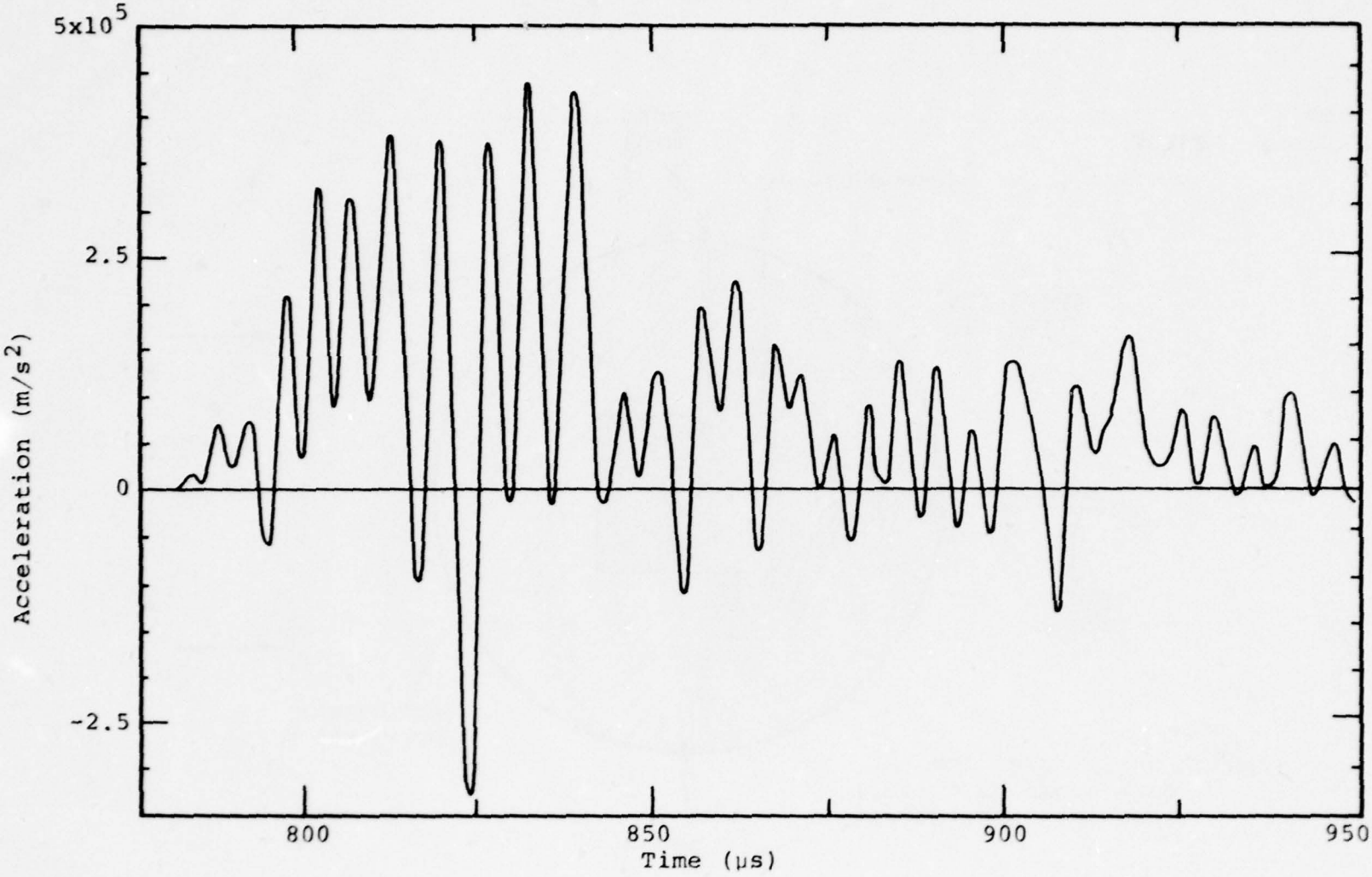

Figure 15. Raw acceleration signal, third shock tube test.

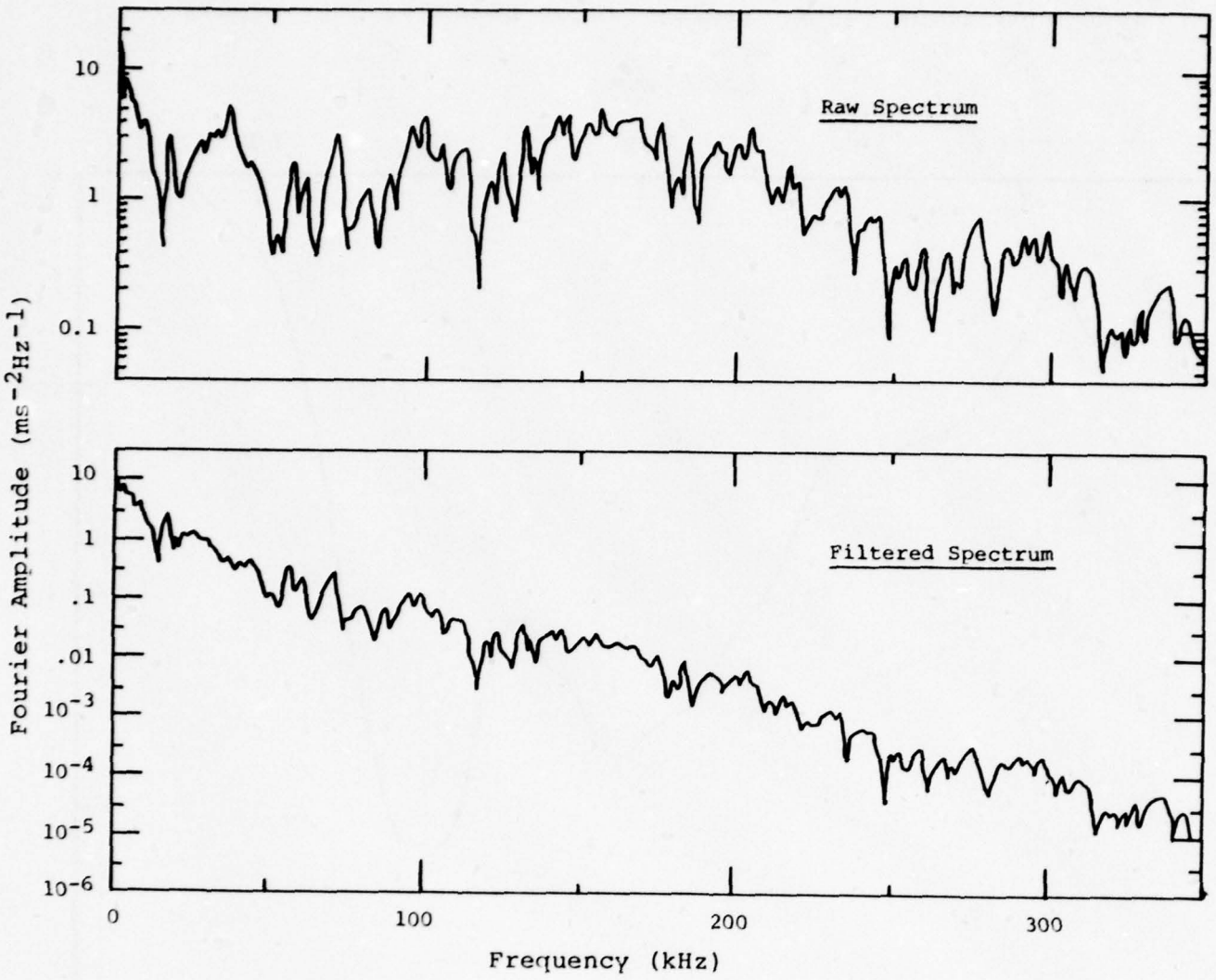

Figure 16. Fourier amplitudes for sphere, third shock tube shot.

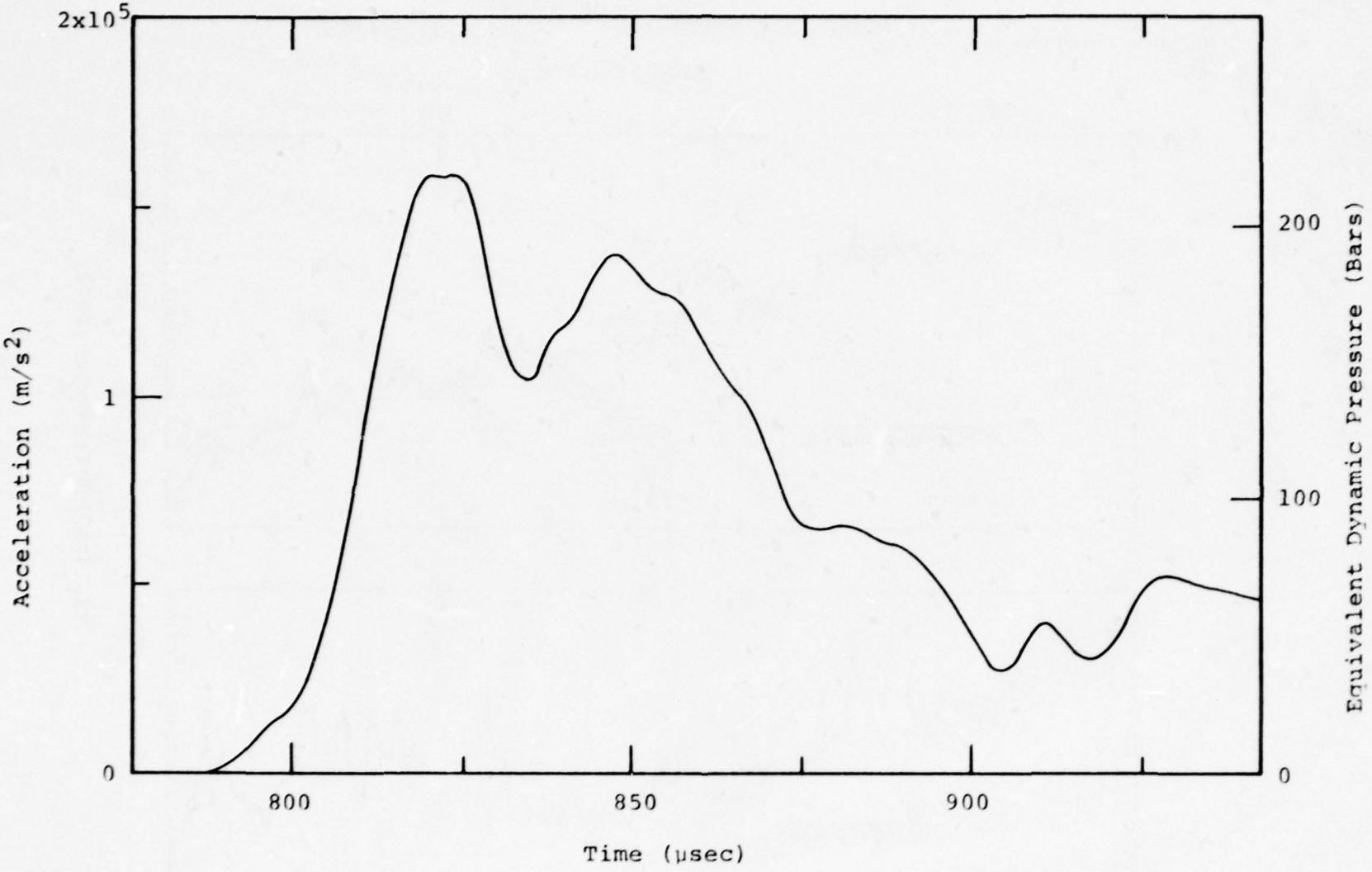

Figure 17. Filtered sphere signal, third shock tube test.

(0.165 kg) of the composite sphere, Equations 20 predict

$$\max a_s = \begin{cases} 1.1 \times 10^5 \text{ m/s}^2 \text{ (Pressure data)} \\ \text{or} \\ 1.4 \times 10^5 \text{ m/s}^2 \text{ (Arrival time data)} \end{cases}$$

This latter value is not far from our "observed" peak of 1.6×10^5 m/s^2.

2.5 CONCLUSIONS

We have completed the initial development of an instrumented sphere to measure dynamic pressure in the supersonic flow behind a blast front. The spheres have operated at static pressure levels of 10^7 Pa (100 bars) and dynamic pressures of ~2×10^7 Pa (200 bars). The shock front excites significant oscillations in the spheres; by the use of a composite structure in the sphere, the magnitude of these vibrations has been greatly reduced. However, more work is needed to further control this problem so that the internal accelerometer is not overranged. If the sphere ringing can be damped, commercially available accelerometers may permit the use of the probe up to dynamic pressures of at least 10^8 Pa (1 kilobar). Additional work is also required to improve the test bed; this would allow a true calibration of the sphere system.

SECTION III

BLAST GAUGES AND MEASUREMENTS

3.1 AIRBLAST GAUGE

A gauge has been designed to measure airblast pressure up to 0.5 GPa (75,000 psi) in underground nuclear tests. The gauge consists of a PCB Model 109A pressure transducer mounted in a massive, hardened steel case and attached to an armored coaxial cable.

The transducer uses a quartz element coupled to a built-in, high gain amplifier to provide a nominal sensitivity of 15 mv/MPa (0.1 mv/psi) and a rise time of 1 μs. The gauge and case are shown in Figure 18 inside a supporting steel sleeve. The sleeve can be fitted over rigid wall electrical conduit and cast into grout at a test site, well in advance of fielding the gauge itself. This is a useful arrangement because the cable connection to the gauge itself cannot be readily fabricated in the field and use of the sleeve permits the gauge and cable assembly to be installed after site construction has been completed. The special connection technique developed for the armored cable has been tested and found to be stronger than the cable itself. The gauge case was hardened to a yield strength of 0.7- 0.8 GPa.

3.2 PRELIMINARY TESTS OF AIRBLAST GAUGE

An effort was made to conduct a test of the blast gauge which would provide a reasonable simulation of the relatively long duration air blast it was designed to measure. Two experiments were performed with the intention of exposing the gauge to a 350 MPa pulse lasting tens of microseconds. In the first test, the gauge was mounted in a small explosive lined cavity in the center of a four foot

SECTION III

BLAST GAUGES AND MEASUREMENTS

3.1 AIRBLAST GAUGE

A gauge has been designed to measure airblast pressure up to 0.5 GPa (75,000 psi) in underground nuclear tests. The gauge consists of a PCB Model 109A pressure transducer mounted in a massive, hardened steel case and attached to an armored coaxial cable.

The transducer uses a quartz element coupled to a built-in, high gain amplifier to provide a nominal sensitivity of 15 mv/MPa (0.1 mv/psi) and a rise time of 1 μs. The gauge and case are shown in Figure 18 inside a supporting steel sleeve. The sleeve can be fitted over rigid wall electrical conduit and cast into grout at a test site, well in advance of fielding the gauge itself. This is a useful arrangement because the cable connection to the gauge itself cannot be readily fabricated in the field and use of the sleeve permits the gauge and cable assembly to be installed after site construction has been completed. The special connection technique developed for the armored cable has been tested and found to be stronger than the cable itself. The gauge case was hardened to a yield strength of 0.7-0.8 GPa.

3.2 PRELIMINARY TESTS OF AIRBLAST GAUGE

An effort was made to conduct a test of the blast gauge which would provide a reasonable simulation of the relatively long duration air blast it was designed to measure. Two experiments were performed with the intention of exposing the gauge to a 350 MPa pulse lasting tens of microseconds. In the first test, the gauge was mounted in a small explosive lined cavity in the center of a four foot

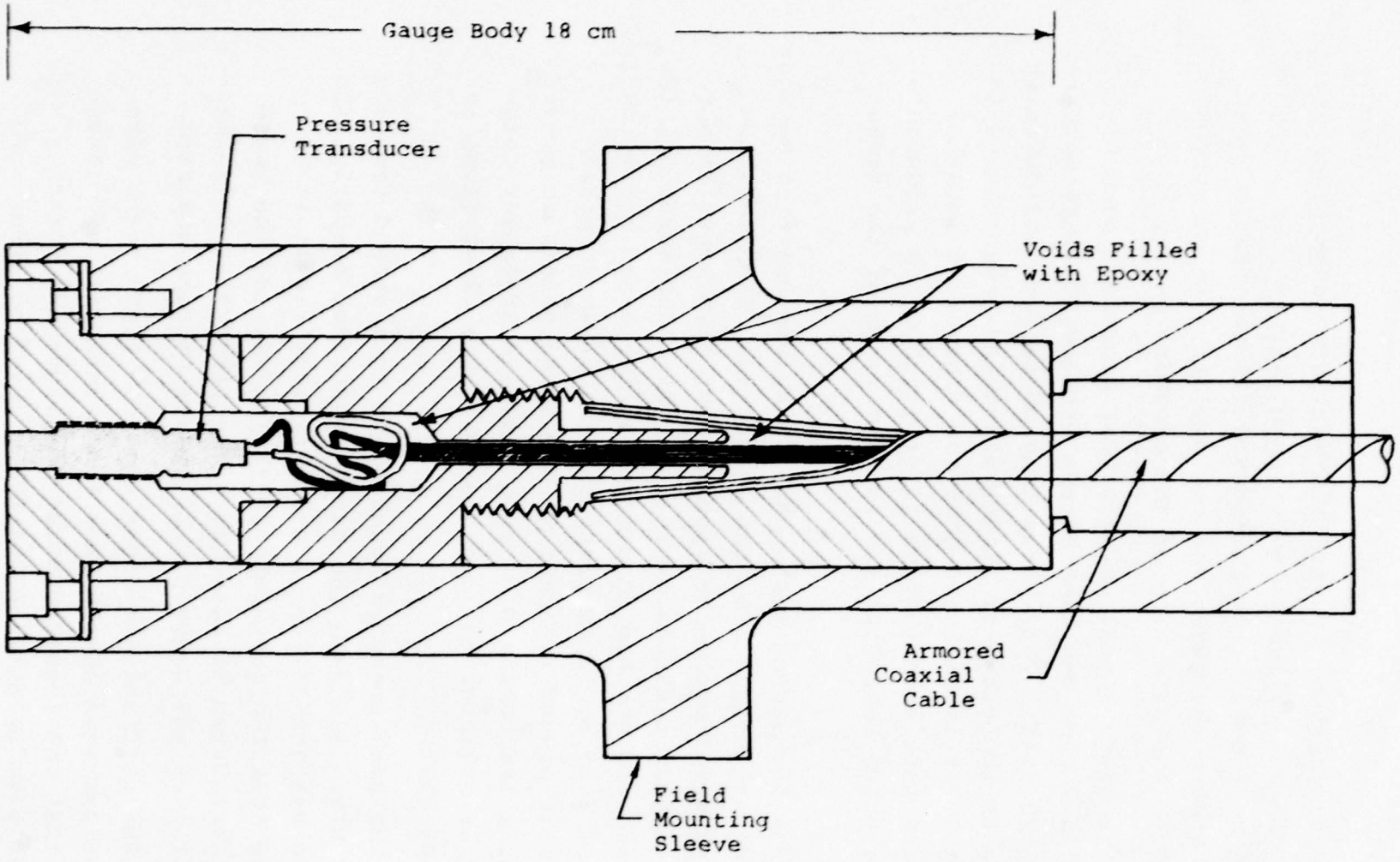

Figure 18. Cross-section view of airblast gauge in field mounting sleeve.

diameter concrete cylinder. The explosive charge was chosen to provide an equilibrium pressure of 500 MPa, assuming complete confinement. A fiberboard filler material was placed between the gauge and the explosive in an attempt to decrease the rise time of the pressure pulse.

The gauge signal in this test reached a peak of 400 MPa in 2 μsec and then became erratic; failure occurred at about 20 μsec. This early time of failure indicates it occurred in the gauge or at the electrical connections to the gauge. It is believed that the fiberboard material compressed into an effective flyer plate which produced a pressure pulse exceeding the maximum range of the transducer.

For the second test, the cavity was modified so that the gauge was offset from the explosive. Five separate layers of sheet explosive spaced about 1 cm apart in air were detonated simultaneously. In this configuration, the explosive products had to pressurize the gauge cavity through a port of 2 cm by 12 cm cross section. Two ytterbium gauges were placed adjacent to the blast gauges to provide a reliable indication of a high pressure transient pulse such as is believed to have destroyed the blast gauge in the first test.

The peak pressure recorded in this second test was only 30 MPa. Although the gauge functioned properly, the pressure was too low to be a significant test. It is possible that the port between the driver and the gauge became obstructed at an early time, preventing full pressurization of the gauge cavity before venting occurred.

The difficulties experienced in these tests were with the pressure source, not the transducer, and it appeared that the required pulse amplitude and duration were not likely to be obtained with the level of effort and

time available for this purpose. Therefore, further small scale testing was suspended in favor of participating in a large scale test to be conducted by the AFWL (see Sections 3.4 and 3.5).

3.3 BAR GAUGES

S^3 was requested to field pressure gauges on the DABS S-2 event in the Have Host test series. To measure pressure in the HE driver chamber, two airblast gauges of the design described above and two long bar gauges were used. The bar gauges were 15.2 m long and consisted of a quartz crystal mounted between equal lengths of 0.635 cm diameter tungsten and aluminum bars; this arrangement provided a recording time of 3.0 ms. In Figure 19 are shown the gauges in the tubular steel housing as fielded, and a detailed drawing of the crystal region.

These gauges were calibrated by using the impact of a steel ball to deliver a measured impulse to the tungsten input bar. A typical gauge signal for such a test is shown in Figure 20. The slight negative undershoot at the tail of the main pulse is believed to be due to the epoxy encapsulation of the sensing crystal, shown in Figure 19. The volume of epoxy used was greater than that used on previous gauges which did not show this effect, and may have resulted in a constraint on the radial expansion of the bar in the region of the crystal. This would effectively increase the impedance of this region and cause a slightly higher signal during the time required for a double transit of a sound wave through this section of the bar (approximately 10 μsec). The crystal would then go into slight tension if the input pulse decayed significantly before the reflection from the end of this high impedance zone reached the crystal. For a long duration pulse this is of no consequence, but for the

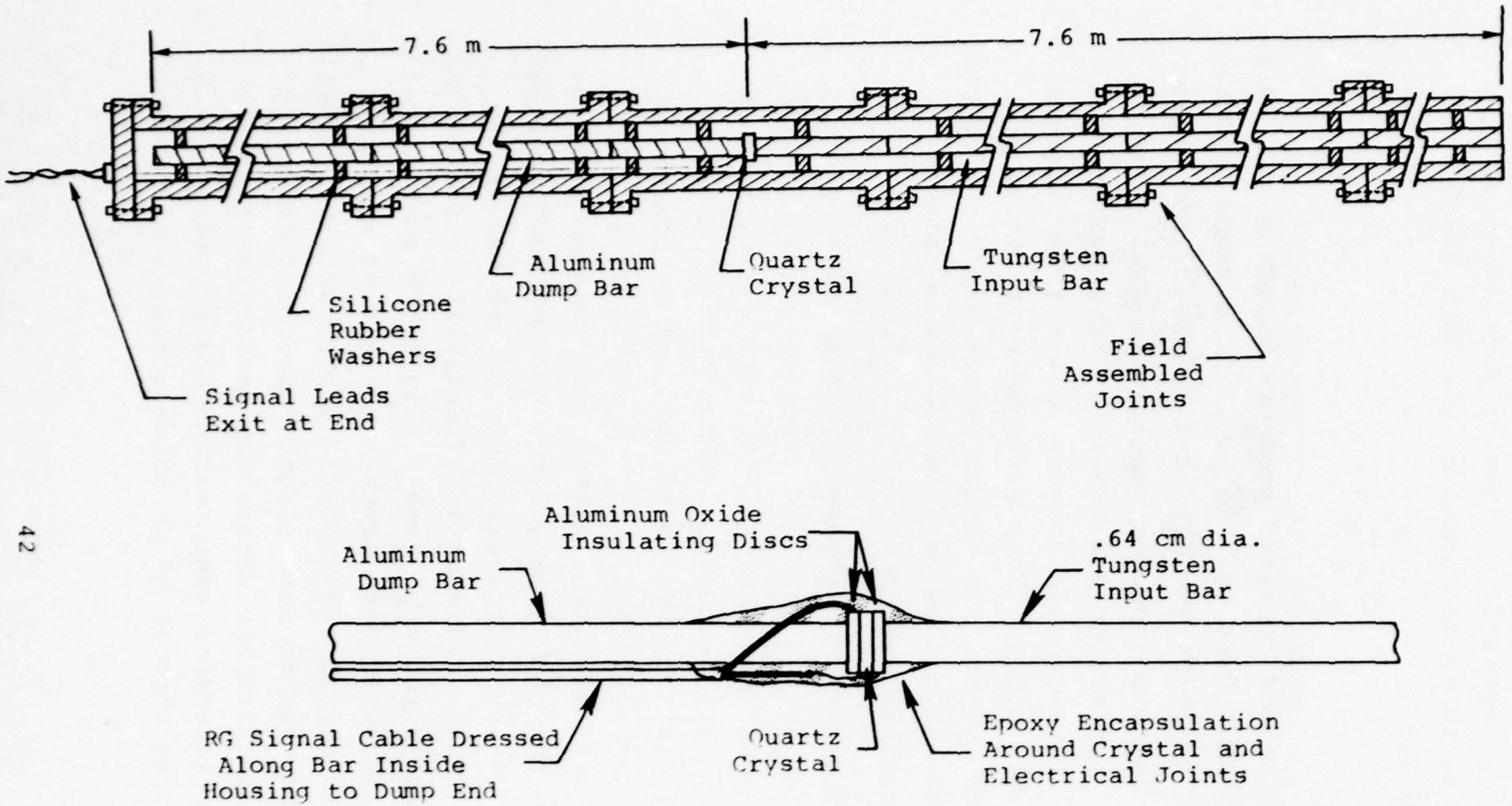

Figure 19. Upper: Bar gauge mounted in support housing.
Lower: Detail of crystal section of bar gauge.

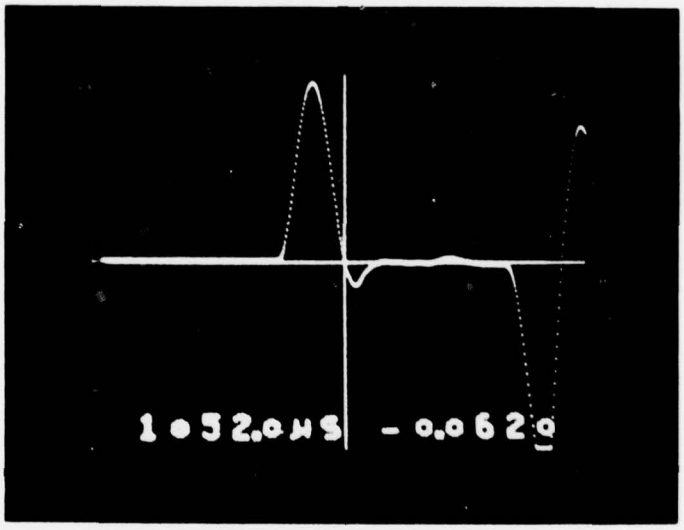

Figure 20. Bar gauge response to short duration impact. (Peak width at baseline is 37 μs).

short pulse delivered by the ball impact (approximately 40 μsec) it caused a significant perturbation. Even in this case, however, the area of the negative peak was only 8% that of the main peak. The air blast from the S-2 test was expected to last on the order of a millisecond, so no modification to the existing gauges was deemed necessary.

3.4 DABS S-2 TEST

The DABS S-2 event in the Have Host series was designed to produce an air blast with a duration of approximately a millisecond. The driver section of the test structure contained blocks of a cast explosive slurry mounted on a vertical wall and a steel plate-covered, reinforced concrete floor. S^3 provided two types of instrumentation on this test: two long bar gauges whose input ends extended through the driver chamber wall to the explosive mounting surface, and two air blast gauges cast into the concrete floor.

The bar gauge location relative to the driver chamber wall is shown in Figure 21. The peak pressure at the wall surface was expected to be slightly in excess of the 1.8 GPa maximum range of the bar gauges. Therefore, a cavity was provided in the explosive around the front ends of the gauges (Figures 22 and 23). The cavity was designed to reduce the peak pressure at the gauge end to approximately 1 GPa. The gauge signal leads exited the bar housing at the rear and were connected directly to battery operated line drivers located near the gauges. This permitted the long cable run to the recording van to be operated at low impedance, greatly reducing the problem of noise pickup.

The air blast gauges were located 1 and 3 meters from the driver chamber wall. Continuous lengths of armored cable connected the transducers to power supplies and line drivers located outside the test structure. Again the

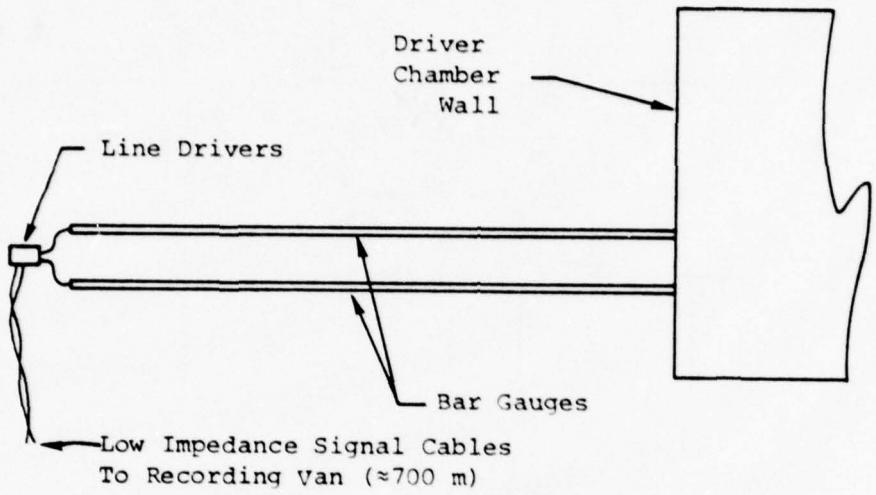

Figure 21. Bar gauge location relative to test chamber (Top View).

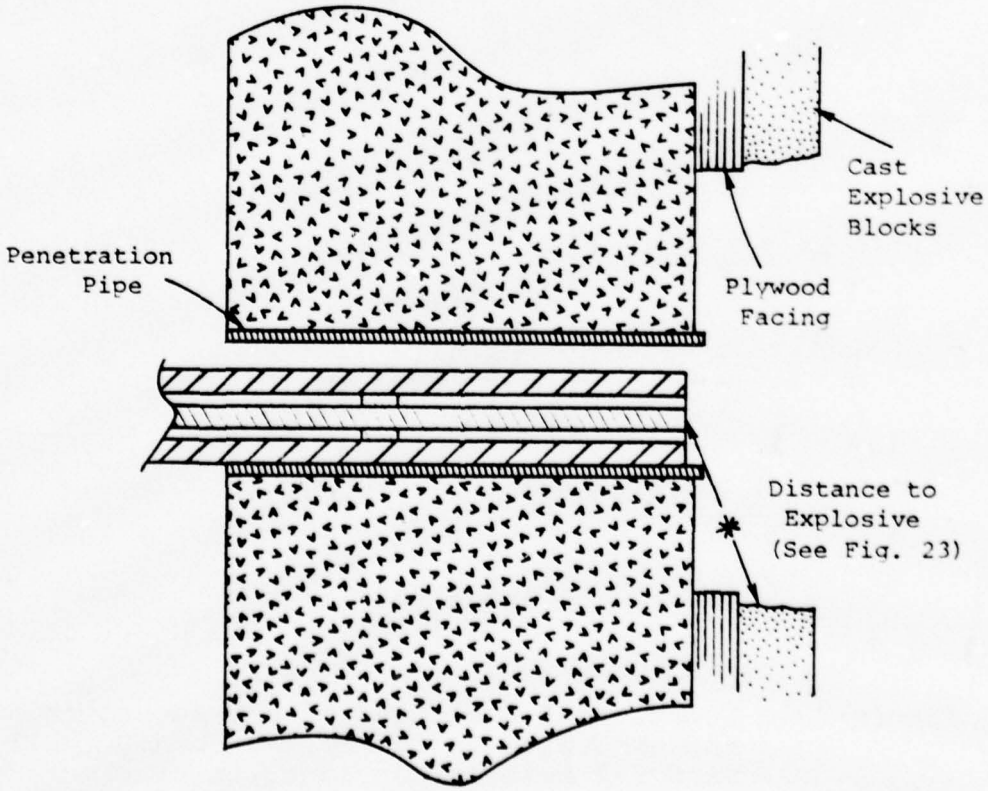

Figure 22. Section through driver chamber wall showing location of bar gauge.

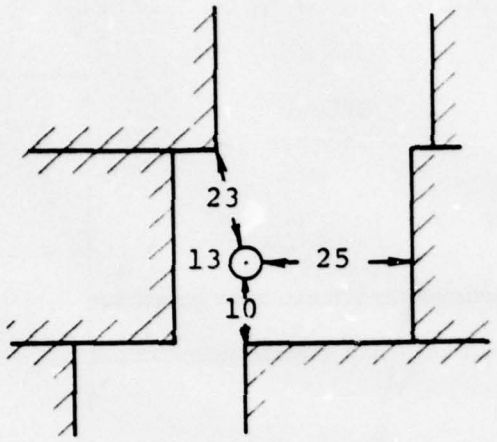

Gauge 9026

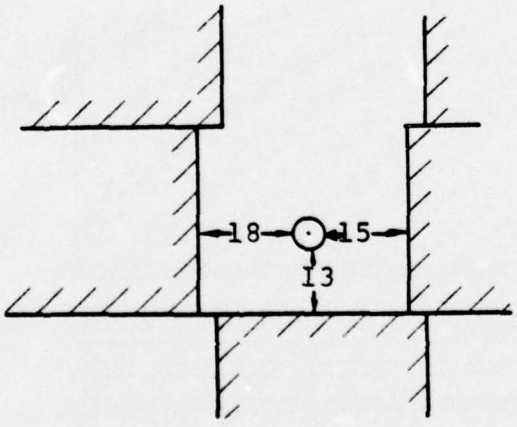

Gauge 9025

Figure 23. Location of input end of bar gauges relative to the explosive on the driver chamber wall on the DABS S-2 test (Dimensions, in centimeters, are not in the plane of the drawing - see Figure 22).

signal conditioning electronics were battery operated to eliminate any problems associated with line voltage stability at firing time.

3.5 RESULTS FROM DABS S-2 TEST

The bar gauges provided good records which indicate a peak pressure of 330 MPa, one third the expected value. The data are plotted in Figures 24 and 25. The zero of the time scale is the firing relay closure time; detonation was initiated approximately 0.8 ms later. The gauge signals start at 2.6 ms, which includes the 1.51 ms propagation time in tungsten input bars. The triple peak structure recorded by gauge 9025 is assumed to be due to the nonsymmetrical arrangement of the explosive blocks relative to the gauge. Gauge 9026 provided a more prominent single peak followed by a series of secondary peaks of approximately 100 MPa, which are believed to be due to the same effect.

A signal reflects off the rear surface of the aluminum dump bar in these gauges and returns to the crystal as a tension wave after a delay of 2.98 ms, the round trip propagation time in the aluminum bar. This tension wave frequently breaks the bond at the crystal, thus terminating the useful recording time of the gauge. The reflection of the initial pressure pulses was clearly recorded by both gauges at 5.75 ms. The large excursion at 6.3 ms recorded by gauge 9026 is believed to be a failure response; however, gauge 9025 indicated a peak at 4.9 ms which is both high in amplitude and considerably longer in duration than the initial peak. This appears to be an actual pressure pulse since the subsequent reflection of the initial signal indicates the gauge was still intact at this time. However, no reflection of this broad signal is seen so it may have been purely electrical in origin. Alternately, it is possible the signal

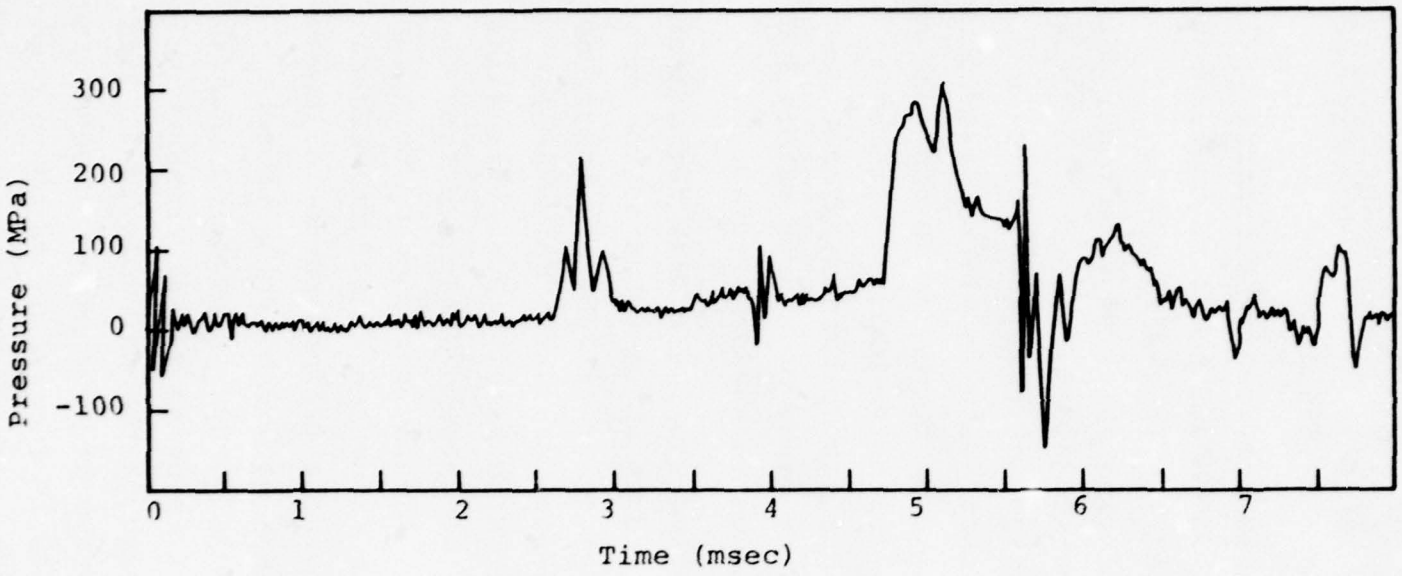

Figure 24. Pressure record from bar gauge 9025 on the DABS S-2 test.

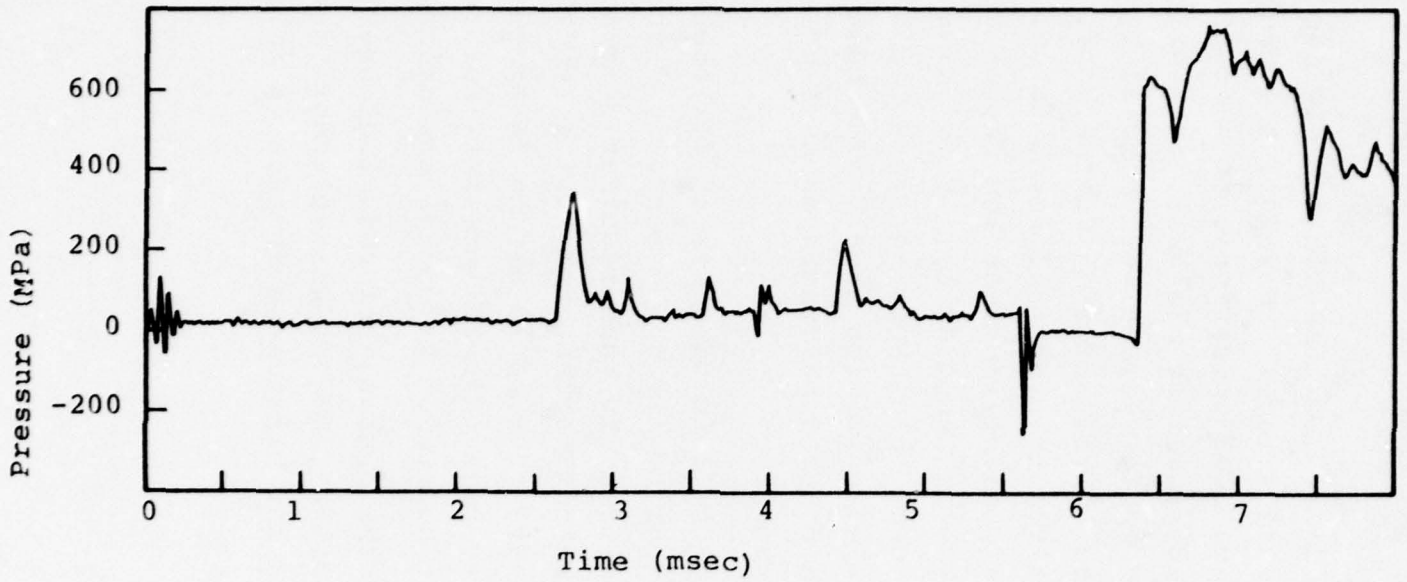

Figure 25. Pressure record from bar gauge 9026 on the DABS S-2 test.

is real and that the gauge had failed before the reflection arrived at the crystal.

No signals whatsoever from the two air blast gauges could be located on the data tapes. However, the gauge systems are believed to have been operational at shot time since, within several hours before the test, the entire transducer, power supply and cable systems were checked by manually applying an impulse to the gauges. Furthermore, both gauges were recovered after the test and found to still be in good condition. The possibility that the gauges could both have been damaged, even temporarily, by the blast, is remote in view of the lower than expected pressure and the fact that at least a brief excursion should have been recorded by the gauges before they could be destroyed by a pulse beyond their pressure range.

A calibration of the recording system for these gauges was made just prior to firing by manually disconnecting the gauge leads from the tape recorder. It is possible that the gauges were not reconnected to the recorder before the shot. However, this could not be determined since the recording system had been changed somewhat (for recalibration) after the test before S^3 personnel could inspect it.

The survival of the gauges, however, indicates that this transducer and housing combination represents a viable technique for obtaining air blast measurements in this type of environment.

SECTION IV

PISTON AND FLUID COUPLING OF BAR GAUGES

4.1 INTRODUCTION

The measurement of static overpressure, stagnation pressure, and the pressure on the surfaces of a double wedge allow many of the flow variables of a strong blast wave to be determined. For example, measurements of static overpressure and stagnation pressure allow the flow-field Mach number to be determined from the following relation (Liepmann and Roshko, 1957):

$$\frac{p_o}{p} = \left(1 + \frac{\gamma-1}{2} M^2\right)^{\frac{\gamma}{\gamma-1}} \qquad (21)$$

where

p_o = stagnation pressure

p = static pressure

M = flow-field Mach number

γ = ratio of specified heats.

This relation is valid for both subsonic and supersonic flow. However, if the stagnation pressure is measured by a stagnation probe, there is a detached shock wave ahead of the probe and the pressure measured by the probe is not the free-stream stagnation pressure. In this case, the following relation (the Rayleigh supersonic pitot formula) must be used to determine the Mach number:

$$\frac{p_m}{p} = \frac{\left(\frac{\gamma+1}{2} M^2\right)^{\frac{\gamma}{\gamma-1}}}{\left(\frac{2\gamma}{\gamma+1} M^2 - \frac{\gamma-1}{\gamma+1}\right)^{\frac{1}{\gamma-1}}} \qquad (22)$$

where

p_m = pressure measured by the stagnation probe in supersonic flow.

Equations (21) and (22) also relate p_m to p_0, the free-stream stagnation pressure.

Having determined the Mach number of the flow from either Equation (21) or Equation (22), its value and the measured static pressure can be used to determine the dynamic pressure of the flow from the following equation:

$$p_d = \text{dynamic pressure} = \frac{\gamma}{2} pM^2 \qquad (23)$$

Measurements of the pressure on the two surfaces of a double wedge (see Figure 26) give information about the flow direction, the ratio of the pressures on the two surfaces being a measure of the flow direction. A plot of the ratio pa/pb versus α (the angle of the incident flow) for various values of the Mach number, shows that the pressure ratio is a sensitive function of α but that it is rather insensitive to the Mach number in the range of interest in underground nuclear tests. The pressure ratio, without additional measurements, would determine α to about $\pm 2°$ during the initial phase of an airblast.

In supersonic flow there is a shock wave near the front of the wedge which may be either attached to the wedge or detached, depending on the wedge angle and the Mach number. It is important for data interpretation that the shock be attached to the wedge. For a Mach 2 flow, this means that

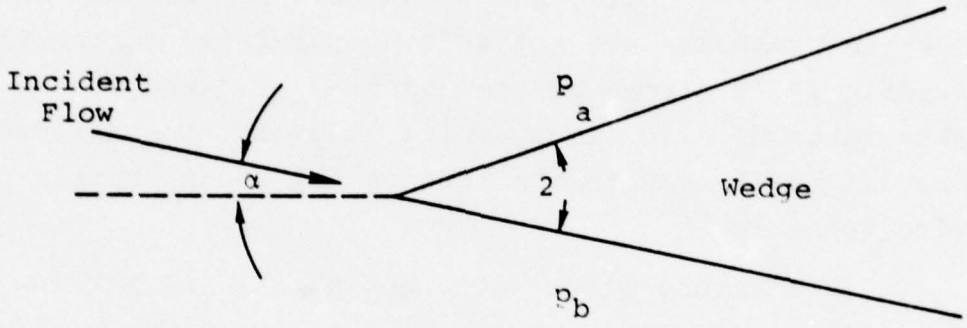

Figure 26. Airflow incident on a double wedge.

for a wedge half angle (θ) of about 10°, the wedge must be aimed to within ±12° of the real flow direction (i.e., $\alpha \leq 12°$). This is a wide enough limit so that one could be fairly confident of being able to properly aim the wedge. If $\alpha > 12°$, the shock will be detached and the observed pressures are not as simply related to the flow direction. If a cone is used instead of a wedge, the acceptable range of α is almost twice as great; the analysis is more difficult than in the case of the wedge, but is still quite feasible.

In a strong blast wave, during the initial few tenths of a millisecond after blast arrival, the flow is strongly supersonic and measurements of wedge or cone pressures can be combined with stagnation or static pressure data to uniquely determine both the Mach number and the dynamic pressure.

In underground nuclear tests, the measurement of static overpressure, stagnation pressure, and pressure on the surfaces of wedges all require instruments to measure pressure versus time in the radiation environment inside the underground cavity. Bar gauges have been used successfully to measure pressure in many underground tests and are well suited for making the measurements considered here. These gauges consist of two long metal rods mounted end-to-end with a quartz or ytterbium stress sensor mounted at the junction of the two rods. One of the rods and the sensor element are imbedded in the cavity wall, primarily to provide protection to the element and the associated electronic circuit from nuclear radiation. The other rod extends into the cavity and transmits the pressure pulse of interest from its exposed end to the sensor.

To measure static overpressure, a slender probe of the type shown in Figure 27 can be used in combination with

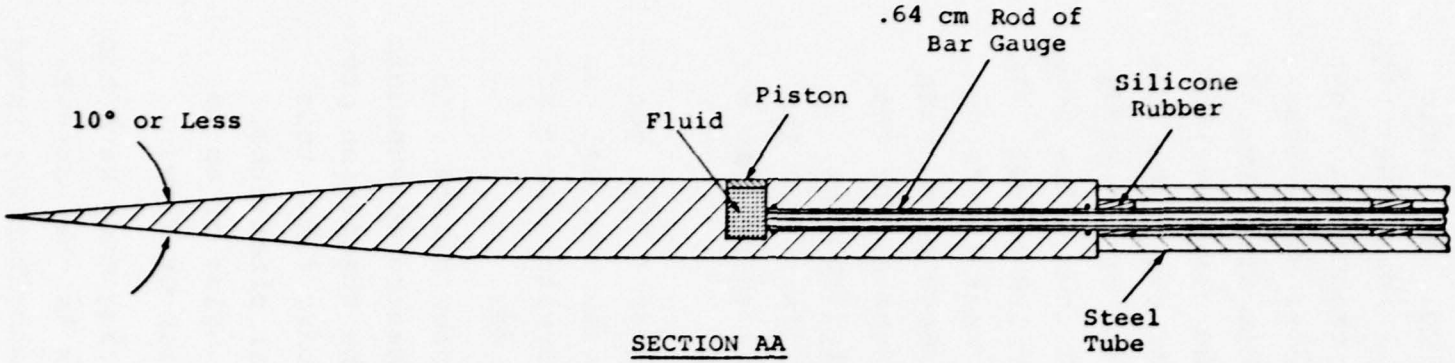

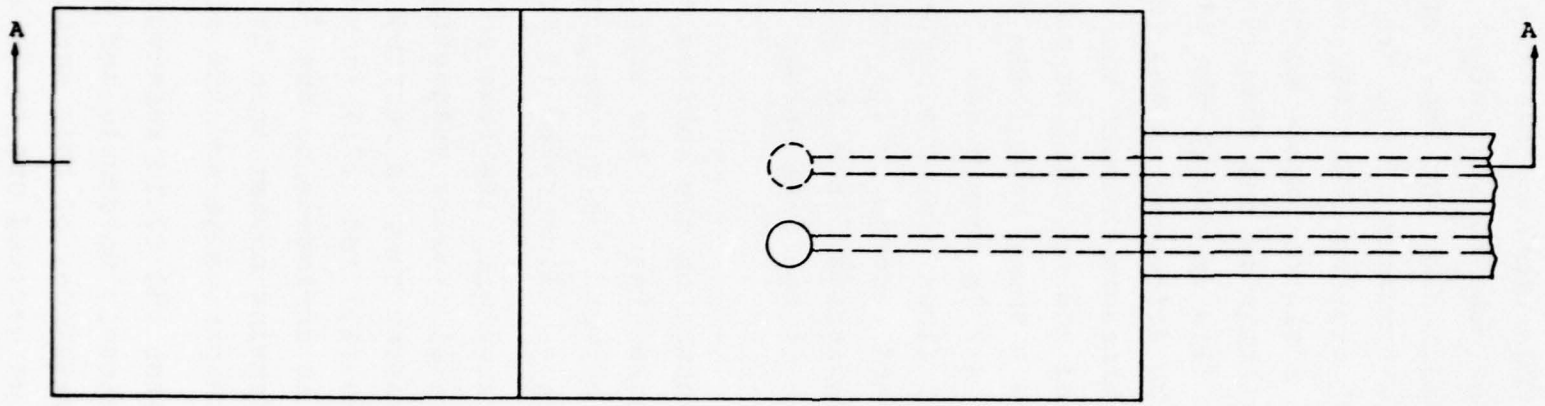

Figure 27. Narrow wedge for measuring static pressure. The pressure is coupled to the bar gauges through fluid filled chambers, with one piston on each side of the straight section beyond the wedge. The bar gauges extend into the cavity wall.

a bar gauge. This probe consists of a narrow wedge (half angle < 10°) followed by a straight section; the static pressure is measured on the faces of the straight section. Pressure on the surfaces of the probe is transmitted to the bar gauges with pistons and fluid reservoirs as indicated in Figure 27. A slender probe such as this disturbs the air flow very little if the flow is in the plane of the probe. If the flow is not in the plane of the probe, the pressure will be different on the two sides of the wedge; measuring the pressure on both sides will thus allow this to be determined and corrections made for its effect. In supersonic flow a shock wave forms at or near the front of the wedge. Air is compressed at the shock wave, then reexpands as it flows over the corner at the end of the wedge section and returns to its original direction. The pressure downstream from the wedge differs from the static pressure of the free stream by less than 1% at M = 2 (Miles, 1950).

The pressure on the surface of wedges (which generally have larger angles than in the static pressure probe) can also be measured with bar gauges combined with piston and fluid couplings as illustrated in Figure 28.

A bar gauge with its free end exposed directly to the air blast will measure stagnation pressure in subsonic flow and a pressure that is related to the stagnation pressure (Equations (21) and (22)) in supersonic flow; this configuration is analogous to the familiar pitot tube. The accuracy remains better than 1% for angles of up to 20° between the bar gauge and the direction of flow.

The piston and fluid reservoir arrangement have not been used previously to couple bar gauges to the pressure source. The remainder of this section describes the investigation that we carried out to determine the risetime and

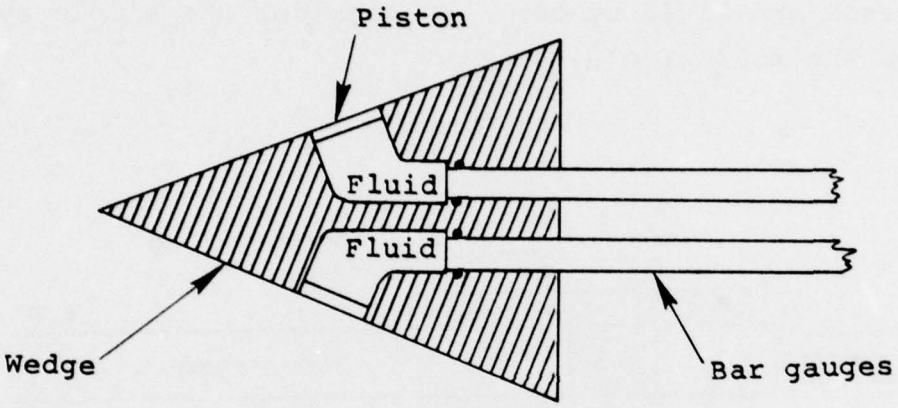

Figure 28. Instrumented wedge for measuring airflow.

response of such piston and fluid coupling systems. The results of these investigations show that such an arrangement would be useful for making measurements in underground nuclear tests.

4.2 ANALYSIS

In this section we calculate approximately the response of a bar gauge that is coupled to the pressure source by a piston and fluid system. We consider the simple system shown in the following diagram:

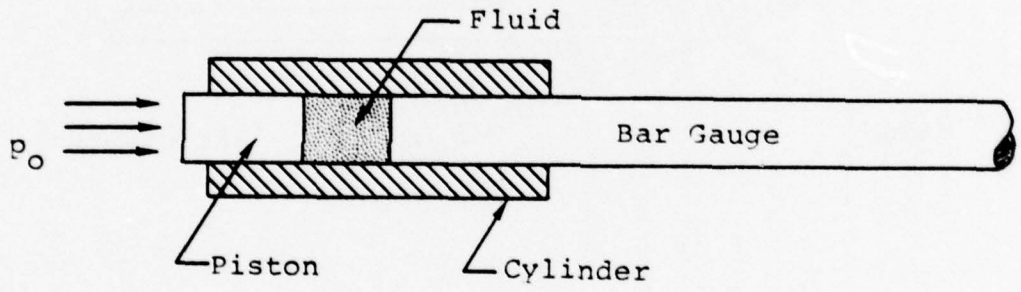

Let p_0 = applied pressure
p_2 = fluid pressure
V = volume of fluid
β = compressibility of the fluid
A = cross-section area of piston and bar
ρ_1 = density of piston
ρ_2 = density of bar
L = length of piston
ℓ = length of fluid reservoir
c_2 = wave velocity in bar
x_1 = displacement of piston
x_2 = displacement of fluid-bar interface

We will not include in the analysis effects of the inertia of the fluid, the friction of the piston nor the viscosity of the fluid. The velocity of the fluid-bar interface is the particle velocity in the bar and is given by

$$u_2 = \text{particle velocity in bar} = \frac{p_2}{\rho_2 c_2} \tag{24}$$

and $$x_2 = \int_0^t u_2 d\tau = \frac{1}{\rho_2 c_2} \int_0^t p_2 d\tau \tag{25}$$

The displacement of the piston is

$$x_1 = x_2 + \frac{\Delta V}{A}$$

But $$\Delta V = \beta V p_2$$

and so $$x_1 = \frac{1}{\rho_2 c_2} \int_0^t p_2 d\tau + \frac{\beta V}{A} p_2 \tag{26}$$

Differentiating gives

$$\frac{dx_1}{dt} = \frac{1}{\rho_2 c_2} p_2 + \frac{\beta V}{A} \frac{dp_2}{dt}$$

and $$\frac{d^2 x_1}{dt^2} = \frac{1}{\rho_2 c_2} \frac{dp_2}{dt} + \frac{\beta V}{A} \frac{d^2 p_2}{dt^2} = \frac{(p_0 - p_2)A}{L\rho_1 A}$$

Rearranging and substituting $V = A\ell$ gives

$$\frac{d^2 p_2}{dt^2} + \frac{1}{\beta \ell \rho_2 c_2} \frac{dp_2}{dt} + \frac{1}{\beta \ell L \rho_1} p_2 = \frac{1}{\beta \ell L \rho_1} p_0 \tag{27}$$

A solution of Equation (27) for p_0 a step function is

$$\frac{p_2}{p_0} = 1 - e^{-t/\tau_1} \left(\cos t/\tau_2 + \frac{2}{\ell} \sin t/\tau_2\right) \tag{28}$$

where $$\tau_1 = 2\beta\ell\rho_2 c_2 \tag{29}$$

and $$\tau_2 = \tau_1\left(\frac{2\rho_2 c_2}{\rho_1 L}\tau_1 - 1\right)^{-\frac{1}{2}} \tag{30}$$

There are other solutions to Equation (27), but Equation (28) is the correct solution for the conditions with piston and fluid coupled bar gauges of interest.

Equation (28) indicates that the pressure p_2 transmitted to the bar gauge is a damped oscillation that approaches the applied pressure p_0, with the time constant τ_1, which depends upon the properties of the fluid and the bar. Since it is desirable to have τ_1 as short as possible, a fluid of low compressibility (e.g., mercury) and a bar of low density (e.g., aluminum) should be used. The length of the fluid reservoir should also be made as small as feasible. The time constant τ_1 also depends upon the wave velocity (c_2) in the bar, but this velocity is not very different for the various materials from which bar gauges might be made. It is interesting to note that τ_1 does not depend upon the density of the piston. However, the oscillation frequency $\frac{1}{2\pi\tau_2}$ does depend upon both the density and the length of the piston.

4.3 DROP BAR TESTS

In order to measure the response of a piston coupled bar gauge, a small fixture incorporating a piston and fluid reservoir was mounted on the end of a bar gauge as shown in Figure 29. The response of the piston and fluid coupling was determined by impacting the piston with a cylindrical drop bar and measuring the output of the bar gauge by recording its signal on an oscilloscope. The drop bar apparatus that was used in these tests was one that had been previously developed for calibrating stress gauges. A drop bar impinging on the end of a bar gauge (without piston and fluid coupling) produces a step function stress pulse in the gauge, the duration of the pulse being twice the acoustic length of the drop bar and the amplitude of the pulse being determined by the velocity of the drop bar. The effect of the piston and fluid coupling on the response of the bar gauge was determined by comparing the output of the bar gauge with the output that would be expected if the drop bar impacted directly on the bar gauge.

The risetime of the stress pulse transmitted to the bar gauge by the piston and fluid is largely determined by the time constant τ_1 in Equation (28), which according to Equation (29) is proportional to the compressibility of the fluid. Since dissolved air or air bubbles in the fluid would increase its effective compressibility (and thereby increase the risetime of the transmitted stress pulse), air was removed from the fluid by treating it in a vacuum. This was accomplished by removing the bar gauge from the fixture, filling the fluid reservoir with fluid, immersing the entire fixture in a beaker of fluid and placing the fluid in a vacuum system. After the fluid had been deaerated (usually after about 15 minutes in the vacuum chamber), the bar gauge was positioned in the fixture and the bleed screw inserted

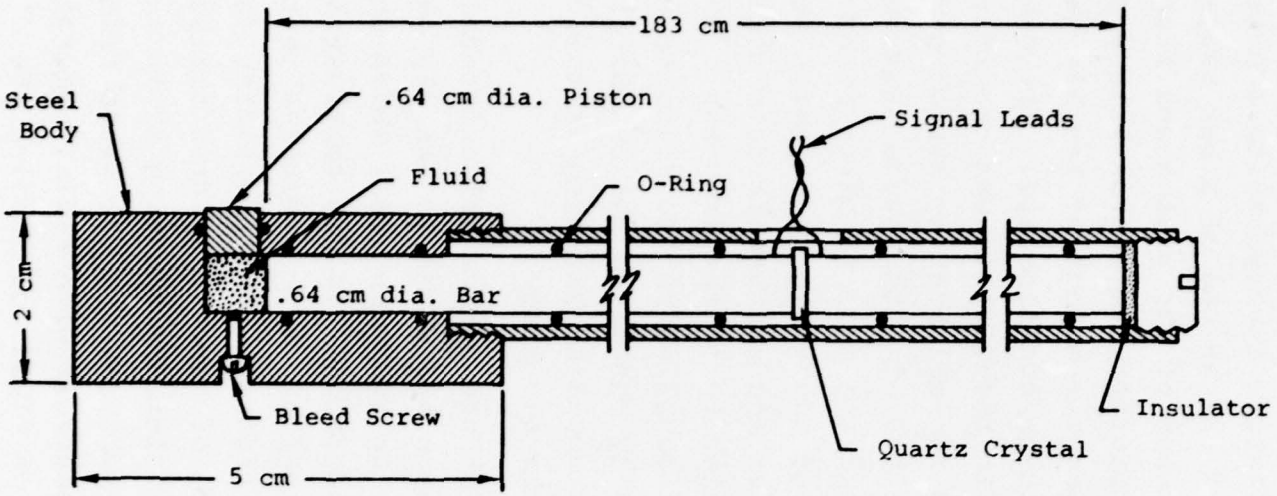

Figure 29. Bar gauge with piston and fluid coupling.

while the fixture was still immersed in the fluid. Fluids that were tested included hydraulic fluid, ethylene glycol and mercury, hydraulic fluid having the highest compressibility and mercury the lowest. Ethylene glycol has about the lowest compressibility of any fluid except mercury.

Equation (29) also shows that the time constant τ_1 is minimized by having the density (ρ_2) of the bar gauge as low as possible. For this reason, bar gauges constructed from both aluminum and steel rods were tested. During the course of these tests it was found that one of the factors that determine the response of the piston and fluid coupling is friction between the piston and the body of the fixture. It was found that lubricating the piston with silicone grease relieved this problem and improved the response. Both neoprene and Teflon O-rings for sealing the piston were tested; the response was about the same with both types, but Teflon O-rings tended to leak more at high pressures than neoprene. Leakage past the O-rings is the problem that limits the maximum pressure at which bar gauges with this coupling arrangement can be used.

Bar gauge signals from tests with hydraulic fluid, ethylene glycol and mercury coupling fluids are given in Figure 30, 31 and 32 respectively. All of these tests were conducted with aluminum bar gauges. These results show that risetime of the stress pulse transmitted to the bar gauge is much shorter with mercury as the coupling fluid than with either hydraulic fluid or ethylene glycol. The compressibility of mercury is only about 10% that of ethylene glycol and the risetime of the signal is seen to be correspondingly reduced.

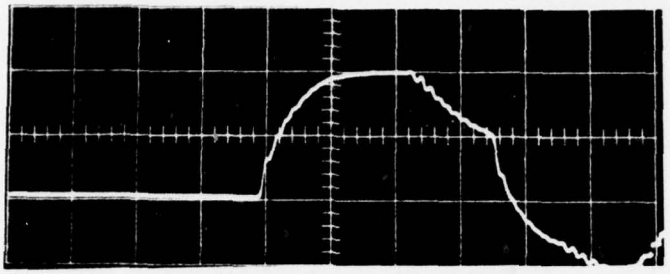

Figure 30. Signal from aluminum bar gauge with hydraulic fluid as the coupling fluid. Vertical scale - 0.25 kbar/cm; sweep speed - 100 μsec/cm.

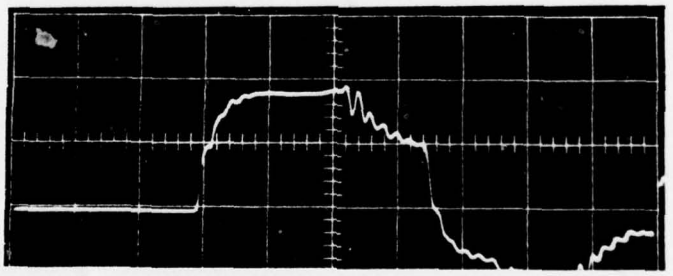

Figure 31. Signal from aluminum bar gauge with ehtylene glycol as the coupling fluid. Vertical scale - 0.25 kbar/cm; sweep speed - 100 μsec/cm.

The signals in Figures 30, 31, and 32 were all from aluminum bar gauges. Figure 33 is the signal from a stainless steel bar gauge with ethylene glycol coupling fluid. Comparing Figures 31 and 33 shows that the risetime increases in about the ratio of the density of the bar gauge material (i.e., 2.7 g/cm^3 for aluminum and 7.8 g/cm^3 for stainless steel), in agreement with Equation (29). The wave velocity c_2 is nearly the same in aluminum and stainless steel (0.51 cm/sec in aluminum and 0.50 cm/sec in stainless steel). In Figure 32, the first drop in the signal at about 230 μs after the onset of the signal was produced by the reflection of the stress pulse from the top end of the 61 cm long drop bar; the second drop in the signal at about 350 μs from the onset of the signal was produced by the reflection from the downstream end of the dump bar in the bar gauge.

The signals in Figures 30, 31, 32 and 33 all show evidence of a damped oscillation starting with the onset of the signal, the frequencies of the oscillations being approximately the frequencies predicted by Equations (28) and (30). However, the amplitude of the oscillations are much lower than predicted by the equations. In developing Equation (28), the friction of the piston, the viscosity of the coupling fluid and the inertia of the fluid were all ignored. It is likely that these all contribute to the observed decrease in amplitude of the oscillations. Including these effects would lead to a very complicated calculation that is not necessary in understanding the important aspects of the piston and fluid couplings.

In Table 3 calculated values of the time constant τ_1 are given for various combinations of coupling fluids and bar gauges. Hydraulic fluid is not included in this table because its compressibility is not known but is thought to be greater than that of ehtylene glycol. The calculated

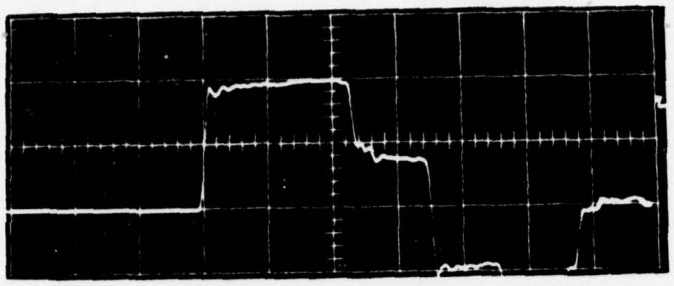

Figure 32. Signal from aluminum bar gauge with mercury as the coupling fluid. Vertical scale - 0.25 kbar/cm; sweep speed - 100 μsec/cm.

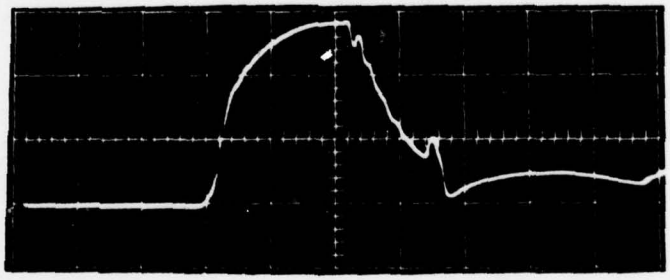

Figure 33. Signal from stainless steel bar gauge with ethylene glycol as the coupling fluid. Vertical scale - 0.25 kbar/cm; sweep speed - 100 μsec/cm.

Table 3. Calculated values of time constant τ_1.

Coupling Fluid	Bar Gauge	β (cm^2/dyne)	ℓ (cm)	ρ_2 (gm/cm^3)	τ_1 (μs)
Ethylene Glycol	Aluminum	4×10^{-11}	0.64	2.7	70
Ethylene Glycol	Steel	4×10^{-11}	0.64	7.8	200
Mercury	Aluminum	4×10^{-12}	0.64	2.7	7

values of τ_1 in Table 3 are seen to be in close agreement with the observed risetime of the signals in Figures 31, 32 and 33. Of particular importance is the calculated and observed fast rise of the signal with the combination of mercury coupling fluid and aluminum bar gauge.

4.4 CONCLUSIONS

The calculations and experiments reported here show that it is feasible to use a bar gauge to measure pressure on a surface parallel to the axis of the gauge by using a piston and fluid coupling combination. This same arrangement can also be used to measure the pressure on a surface positioned at any angle relative to a bar gauge. The best response was achieved with the combination of mercury as the coupling fluid and an aluminum bar gauge. It is important that all air be removed from the fluid by treating it in a vacuum when the fluid coupling and bar gauge are assembled.

Although the coupling arrangement was not tested in a blast wave, it should be useful for measuring the pressure on the surfaces of wedges exposed to blast waves in underground nuclear tests. However, before being used in nuclear tests it is recommended that such wedge measurements be tested in an explosively driven shock tube. One of the main problems encountered was friction between the piston and the wall of the hole in which the piston was located. This problem could probably be relieved by lining the hole with a Teflon sleeve in which the piston would be located. Such an arrangement should be tested in a shock tube to make sure that the blast pressure does not compress the Teflon sleeve and cause binding of the piston. It is likely, however, that piston friction will be less of a problem when the pressure is applied by a blast wave instead of by a drop bar because the pressure will be applied more uniformly over the area of the piston.

SECTION V
THERMAL RADIATION DETECTOR

5.1 INTRODUCTION

The thermal radiation due to air blast and the fire ball of a nuclear explosion is an important effect. The magnitude and spectral distribution of this energy flux are sensitive monitors of the accuracy of calculations that try to describe the explosion. In an air blast, the total energy in thermal radiation is about 40% of the total device yield, while the visible light energy is about 25% of the yield. These values are functions of the depth of burial, probably being considerably reduced by even shallow burial. For these reasons, it is desirable to measure the time variation of the total thermal radiation in certain underground nuclear tests.

A heat transfer gauge that was successfully fielded by S^3 on HYBLA FAIR (Kratz, 1975) can be adapted to measure the total radiative flux in a nuclear tests. This gauge consists of a thermally isolated thin copper disc, the front face of which is exposed to the radiation; a platinum resistance element measures the temperature rise of the back face of the disc. To determine the radiative flux incident on the front surface of the disc, the temperature history measured at the back surface is compared with results of numerical heat flow calculations (using an S^3 heat conduction code) for given flux histories on the front surfaces. The incident flux used as input to the calculation is adjusted until the calculated temperature history at the back surface of the disc agrees with the measured temperature history. For a properly blackened front surface, the gauge will respond to all wavelengths over all angles of incidence; i.e., it is a bolometric detector sensitive over 2π steradians.

The platinum resistance element is electrically insulated from the back surface of the disc by a vapor deposited, 2 micron thick layer of sapphire. This thickness of sapphire, if the layer is free of pinholes, is sufficient to provide the necessary electrical insulation between the platinum resistance element and the copper disc, but also it is thin enough that the thermal time lag between the back surface of the disc and the resistance element is only a few microseconds. The platinum resistance element is evaporated on top of the sapphire layer and electrical leads are attached to it with conducting epoxy. The circuitry for this gauge is similar to that used in manganin and ytterbium stress gauges. The platinum resistance element is made one arm of a pulsed bridge circuit which is located in an instrument alcove or in the recording trailer. The resistance of the element increases as its temperature increases, thus producing an unbalanced bridge voltage whose magnitude is related to the temperature rise.

Although this gauge was successfully fielded on HYBLA FAIR, there were difficulties in producing pinhole free sapphire insulating layers on the back surfaces of the copper discs. The sapphire was vacuum deposited by evaporation, but many of the samples that were made by this technique contained pinholes. Such pinholes caused the platinum resistance element, which was subsequently evaporated on top of the sapphire layer, to be shorted to the copper disc, thereby rendering the sample useless. A large number of samples were fabricated in order to obtain six pinhole free layers for use in the HYBLA FAIR gauges. The pinhole problem was considered to be the most important problem to be solved in developing a radiation detector. To help solve this problem, S^3 retained a consultant, Dr. Lee Donaghey, Berkeley, California, who is an expert in thin film technology. It was his opinion

that it would be easier to produce pinhole free sapphire layers by sputtering than by evaporation. His attempts to produce pinhole free sapphire layers using the sputtering technique are described in the remainder of this section.

5.2 SPUTTERING EXPERIMENTS

In the sputtering process, sapphire (Al_2O_3) is produced by oxidizing aluminum atoms that are removed from an aluminum target. This is done by generating a plasma between an aluminum target and a conducting ground plane to which the object to be coated is attached. A low pressure gas containing oxygen fills the space between the target and the ground plane. The plasma is generated by applying a high voltage between the target and the ground plane.

In the experiments conducted in support of this program, the sputtering apparatus consisted of a vacuum system with an aluminum bell jar, a 6-inch diameter pure aluminum target, a steel ground plane, and a gas consisting of a mixture of filtered argon and oxygen, the percentage of oxygen in the mixture being variable. Various substrates on which sapphire was deposited included 2-inch diameter polished copper discs, glass slides, quartz cover slides, titanium discs and optically polished silicone. Experiments were conducted in which the amount of oxygen in the gas mixture was varied from zero to 2%, the gas pressure was varied from 10 to 20 mTorr, and the voltage was varied between 720 and 1000 volts.

The results of this series of experiments are summarized as follows:

1. The deposition rate depends on the oxygen partial pressure in the plasma. With less than 1% oxygen the deposition rate is high and the deposited layer is optically colored, usually deep blue. With greater

than 1% oxygen the deposition rate is low and the sapphire layer is white or slightly orange in color.

2. The conductivity of the deposited layer also depends on the partial pressure of oxygen. With less than 1% oxygen a semiconducting layer of sub-oxide is deposited; with more than 1% oxygen a strict-oxide insulating layer is deposited. The sub-oxide to strict-oxide transition is at the same partial pressure of oxygen as the color transition.

3. If the sputtering power is greater than 250 watts with a 6-inch diameter target, the temperature rise is sufficient to oxidize the surface of a copper substrate. Such an oxide layer weakens the adhesion of the sapphire film.

4. Diffusion of copper into the sapphire film reduces the resistivity of the sapphire film and also tends to produce a mottled film.

5. Contamination of the plasma by extraneous materials must be kept to an absolute minimum. Sputtering up, i.e., with the ground plane and substrate above the target, prevents particulate matter from adhering to the substrate surface.

6. The preparation of the surface of the copper is one of the most important considerations, but also one of the most difficult, in producing pinhole free, strongly adherent sapphire films. This surface must be as smooth and free of contaminants as possible. A true optical finish cannot be obtained on copper, but residual scratches must be less than 1 micron.

The experimental sputtering program did not advance to the point where pinhole free, strongly adhering sapphire films on copper could be produced on a routine basis. However, sufficient work was done to indicate that the production of such films is feasible. The one problem area that requires additional work is the preparation of the copper surface on which the sapphire film is deposited. An extremely clean sputtering system is a necessity and it will probably be necessary to devote a system entirely to this process. Once the sapphire film problem is adequately solved, completing the development of the thermal radiation gauge should be straightforward.

REFERENCES

1. American Institute of Physics Handbook, Third Edition, D. E. Grey, ed. (1972), McGraw-Hill.

2. Bailey, A. B. and J. Hiatt (1971), "Free-Flight Measurements of Sphere Drag at Subsonic, Transonic, Supersonic and Hypersonic Speeds for Continuum, Transition and Near-free-molecular Flow Conditions," Arnold Engineering Development Center, AEDC-TR-70-291.

3. Cavaliere, A. and A. Messina (1976), "Propagation of Blast Waves," Astrophysical Journal 209, 424.

4. H. R. Kratz (1975), "HYBLA FAIR Event, Diagnostic Measurements," Systems, Science and Software Report No. SSS-R-75-2631 (DRAFT).

5. H. W. Liepmann and A. Roshko (1957), Elements of Gasdynamics, Wiley, New York.

6. A. E. H. Love (1944), A Treatise on the Mathematical Theory of Elasticity, Fourth Edition, Dover.

7. E. R. C. Miles (1950), Supersonic Aerodynamics, Dover Publications, Inc.

DISTRIBUTION LIST

DEPATMENT OF DEFENSE

Assistant to the Secretary of Defense
Atomic Energy
ATTN: Executive Assistant

Defense Advanced Rsch. Proj. Agency
ATTN: TIO
ATTN: NMRO
ATTN: PMO
ATTN: STO

Defense Documentation Center
Cameron Station
12 cy ATTN: TC

Defense Nuclear Agency
ATTN: SPSS
ATTN: DDST
ATTN: SPTD
4 cy ATTN: TITL

Field Command, Defense Nuclear Agency
ATTN: FCTMOF
ATTN: FCT
ATTN: FCPR

Livermore Division, Field Command, DNA
Lawrence Livermore Laboratory
ATTN: FCPRL

Under Sec. of Defense for Rsch. & Engrg.
ATTN: Strategic & Space Systems (OS)

DEPARTMENT OF THE ARMY

Deputy Chief of Staff for Rsch. Dev. & Acq.
ATTN: DAMA-AOA-M

Harry Diamond Laboratories
ATTN: DELHD-NP
ATTN: DELHD-TI

U.S. Army Ballistic Research Labs.
ATTN: DRDAR-BLE, J. Keefer
ATTN: DRXBR-X, J. Meszaros
ATTN: Technical Library

U.S. Army Engr. Waterways Exper. Sta.
ATTN: Library
ATTN: L. Ingram
ATTN: W. Flathau
ATTN: F. Hanes

U.S. Army Materiel Dev. & Readiness Cmd.
ATTN: DRXAM-TL

DEPARTMENT OF THE NAVY

Office of Naval Research
ATTN: Code 715

Civil Engineering Laboratory
Naval Construction Battalion Center
ATTN: Code L08A
ATTN: R. Odello

DEPARTMENT OF THE NAVY (Continued)

David W. Taylor Naval Ship R&D Ctr.
ATTN: L42-3

Naval Facilities Engineering Command
ATTN: Code 09M22C

Naval Ship Engineering Center
ATTN: Code 09G3

Naval Surface Weapons Center
ATTN: Code F31

DEPARTMENT OF THE AIR FORCE

AF Geophysics Laboratory, AFSC
ATTN: Research Library

AF Institute of Technology, AU
ATTN: Library

AF Weapons Laboratory, AFSC
ATTN: DEX, J. Renick
ATTN: DES-S, M. Plamondon
ATTN: SUL
ATTN: DEX

Assistant Chief of Staff, Intelligence
ATTN: INATA

DEPARTMENT OF ENERGY

Department of Energy
Albuquerque Operations Office
ATTN: Doc. Con. for Technical Library

Department of Energy
ATTN: Doc. Con. for Classified
Technical Library

Department of Energy
Nevada Operations Office
ATTN: Doc. Con. for Technical Library

Lawrence Livermore Laboratory
ATTN: Doc. Con. for Technical Information
Dept. Library

Oak Ridge National Laboratory
Union Carbide Corporation-Nuclear Division
ATTN: Doc. Con. for Mr. Kearny

Sandia Laboratories
Livermore Laboratory
ATTN: Doc. Con. for Library &
Security Classification Div.

Sandia Laboratories
ATTN: Doc. Con. for A. Chaban
ATTN: Doc. Con. for L. Vortman
ATTN: Doc. Con. for 3141

OTHER GOVERNMENT AGENCY

National Bureau of Standards
ATTN: P. Lederer

DEPARTMENT OF DEFENSE CONTRACTORS

Aerospace Corp.
ATTN: P. Mathur
ATTN: Technical Information Services

Agbabian Associates
ATTN: M. Agbabian

Artec Associates, Inc.
ATTN: D. Baum

Civil/Nuclear Systems Corp.
ATTN: J. Bratton

EG&G Washington Analytical Services Center, Inc.
ATTN: Library

Electromechancial Sys. of New Mexico, Inc.
ATTN: R. Shunk

General Electric Co.-TEMPO
Center for Advanced Studies
ATTN: DASIAC

H-Tech Laboratories, Inc.
ATTN: B. Hartenbaum

IIT Research Institute
ATTN: Documents Library

Kaman Sciencies Corp.
ATTN: Library
ATTN: D. Sachs

Merritt CASES, Inc.
ATTN: J. Merritt

Nathan M. Newmark
Consulting Services
ATTN: W. Hall

Physics International Co.
ATTN: F. Sauer/C. Godfrey
ATTN: C. Vincent
ATTN: Technical Library

R&D Associates
ATTN: Technical Information Center
ATTN: C. Knowles/J. Lewis

DEPARTMENT OF DEFENSE CONTRACTORS (Continued)

Science Applications, Inc.
ATTN: Technical Library

Southwest Research Institute
ATTN: A. Wenzel

SRI International
ATTN: G. Abrahamson
ATTN: B. Gasten/P. De Carli

Systems, Science & Software, Inc.
ATTN: D. Grine
ATTN: Library
ATTN: H. Kratz
ATTN: P. Coleman
ATTN: R. Wilson

TRW Defense & Space Sys. Group
ATTN: Technical Information Center
2 cy ATTN: P. Dai

TRW Defense & Space Sys. Group
San Bernardino Operations
ATTN: F. Wong

The Eric H. Wang
Civil Engineering Rsch. Fac.
ATTN: N. Baum

Weidlinger Assoc.
Consulting Engineers
ATTN: M. Baron

Weidlinger Assoc.
Consulting Engineers
ATTN: J. Isenberg